Fluorine Conformational Effects Characterized by Energy Decomposition Analysis

Natalia Díaz,* Fernando Jiménez-Grávalos, Dimas Suárez, Evelio Francisco, and Ángel Martín-Pendás

Departamento de Química Física y Analítica. Universidad de Oviedo. Avda. Julián Clavería 8, 33006 Oviedo (Asturias). Spain.

diazfnatalia@uniovi.es

Abstract

Electrostatic and stereoelectronic effects associated to fluorine atoms can be exploited as conformational tools for the design of shape-controlled functional molecules. To gain further insight into the nature and strength of these effects, we use the Interacting Quantum Atoms (IQA) method augmented with the semiclassical pairwise dispersion potential to decompose the conformational energies of fluoro-substituted molecules into fragment-based energy contributions, which include deformation/distortion terms and the electrostatic, exchange-correlation and dispersion interactions. The studied molecules comprise various $F-CH_2-CH_2-X$ and $F-CH_2-CO-X$ systems, as well as selected conformers of an α,β-difluoro-γ-amino-acid derivative that is potentially useful for the design of shape-controlled bioactive amino acids and peptides. We identify the most relevant exchange-correlation and/or electrostatic interaction terms contributing to the stability of the various conformers, and we show that IQA can assess the *gauche/anti* or *trans/cis* preferences in molecules with two or more rotatable bonds as well as to study the roles played by other concomitant effects (*e.g.*, CH/OH/NH$\cdots$F contacts). For the α,β-difluoro-γ-amino acid derivatives, our theoretical analysis points out that the *gauche/anti* and *trans/cis* effects associated to fluorine bonds can be significantly attenuated by other specific intra-molecular contacts.

Introduction

In the last decades, fluorine has arisen as a remarkable element in numerous applications. Some of the most successful drugs on the market today include one or more fluorine atoms in their structures. Fluorine-containing molecules have made a significant contribution to the development of modern crop protection agrochemicals (herbicides, insecticides, and fungicides).[2, 3] Fluorinated materials are widely used in liquid crystal displays[4] and in photovoltaic solar cells.[51] Specific fluorine substitution redefines the reactivity of non-fluorinated substrates and catalysts in terms of reaction yields, diastereo- or enantiomeric ratios, and mechanistic pathways.[6, 7] Similarly, fluorination modifies hydrophobicity, ring puckering and secondary structure propensity of amino-acids, and influences peptide/protein folding, stability and intermolecular interactions.[8]

The introduction of fluorine into a molecule can affect different physicochemical properties (*i.e.* hydrophobicity, reactivity, conformation, noncovalent interactions, etc.) due to electrostatic and stereoelectronic effects. Fluorine is a small atom that can replace hydrogen in organic molecules with a minimal steric impact, but with significant electronic consequences. It is the most electronegative element and, accordingly, the C−F bond presents a high polarity (*i.e.* $C^{\delta+}-F^{\delta-}$) and a low polarizability. This results in a strong ionic character and a large dipole moment for the C−F moiety that influence the chemical properties of adjacent groups.[9] For example, pK_a values of acetic acid and its successive α-fluorinated derivatives change from 4.76 (CH_3COOH) to 0.23 (CF_3COOH) upon fluorine substitution.[10] In addition, numerous examples show that stereoselective introduction of fluorine atoms within a molecule results in different conformational properties.[11-15] On one hand, the C−F bond tends to align antiparallel to adjacent C=O bonds to confront the corresponding dipole moments,[11] and to orient itself close to positively charged groups in order to maximize favorable charge/dipole interactions.[16] On the other hand, the high electronegativity of fluorine determines the presence of a low energy σ^{*}_{C-F} antibonding orbital that can accommodate electron density from stereoelectronically aligned lone pairs or adjacent σ and π bonds. Although this stereoelectronic effect (hyperconjugation) is energetically small, it has been traditionally invoked to explain the stabilization of certain molecular conformations.[9]
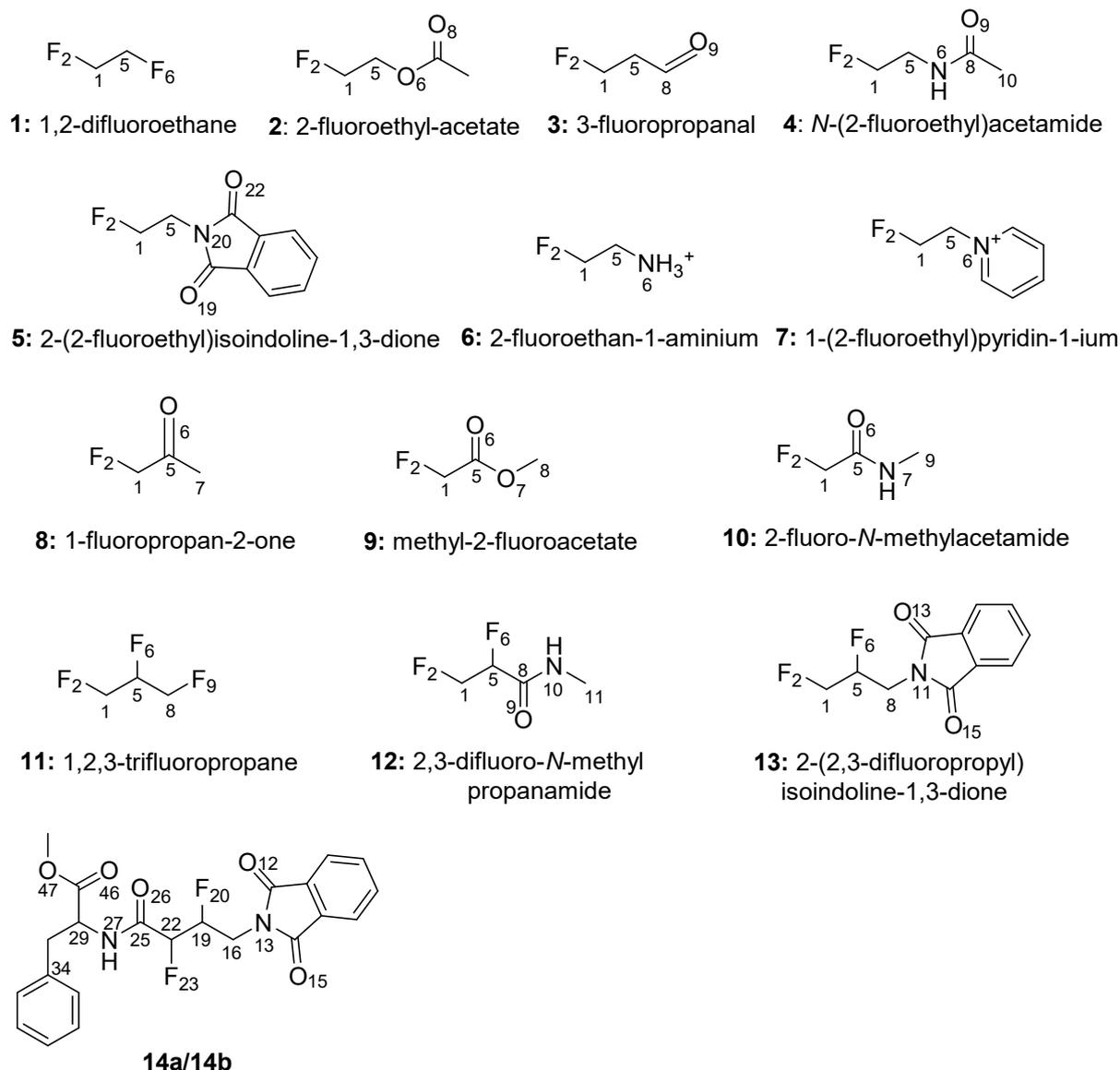
Traditionally, 1,2-difluoroethane has been considered the benchmark case for understanding the origin of the *gauche* structural preference (*i.e.* F-C-C-X angle around 60º).

In previous computational works,[17-19] the natural bond orbital (NBO) method[20] ascribes the *gauche* preference in 1,2-difluoroethane to the $\sigma_{CH} \rightarrow \sigma_{CF}^{*}$ hyperconjugative interactions arising when adjacent C-H and C-F bonds align antiparallel. However, the ability of NBO to provide a right balance between Lewis (*i.e.* steric and electrostatic) and non-Lewis contributions has been questioned[21] by the Energy Decomposition Analysis (EDA) approach,[22] which similarly dismisses the central role of hyperconjugation in the conformational *gauche* effect. Thus, when EDA characterizes the interaction between two CH_2F radicals in the *gauche/anti* geometries of 1,2-difluoroethane, it turns out that equally-favorable orbital and electrostatic interactions contribute to explain the *gauche* effect.[23] Further support for the role of electrostatic interactions comes from an Interacting Quantum Atoms (IQA) analysis, in which the largest diatomic contribution to *gauche* stability is provided by the electrostatic interaction between carbon and fluorine atoms in positions 1,3.[24] As a result, the authors conclude that the origin of the *gauche* effect in 1,2-difluoroethane is electrostatic rather than hyperconjugation.

Besides 1,2-difluoroethane, the conformational effects associated to the presence of fluorine atoms have been computationally analyzed in related compounds. For instance, DFT energy profiles connecting the *gauche* and *anti* conformers and atomic charges have been evaluated for a series of 16 β-substituted α-fluoroethanes ($F-CH_2CH_2-X$) in order to assess the influence of steric and electrostatic interactions, meanwhile NBO analysis are employed to disclose the role of hyperconjugation.[18] These results point out that both electrostatic and hyperconjugative effects may contribute to conformer stability. In general, the role of hyperconjugation stabilizing the *gauche* structures increases with the electronegativity of the first atom in the X moiety. Favorable electrostatic interactions between fluorine and electropositive atoms in the X substituent also contribute to the *gauche* preference, with a remarkable *gauche* stabilization observed for positively charged groups like in 2-fluoroethylammonium ($F-CH_2CH_2-NH_3^+$).[16, 18, 25] It has been also found that F atoms adjacent to carbonyl groups stabilize the *trans/gauche* F-C-C=O arrangements in the gas-phase, although this intrinsic preference can be reversed to the alternative *cis* form in polar solvents as suggested by DFT calculations coupled with a continuum solvent model.[26-28] On the other hand, the NBO characterization of the 2-fluoroethanol ($F-CH_2CH_2-OH$) conformers has explained the largest stability of a particular *gauche* structure by the presence of a favorable electrostatic $O-H^{\delta+}\cdots^{\delta-}F$ interaction, which is termed as a non-classical hydrogen bond.[29] In contrast, a very recent work interprets the $^4J_{HF}$ couplings in α-fluoro amides as a genuine N-

H···F hydrogen bond.[30] Finally, the *anti/gauche* conformers around the F-C-C-S sequence in sulfur-containing systems have been subject to EDA considering the $FH_2C\cdot$ and $\cdot CH_2SX$ radicals as reference fragments.[31] The electrostatic interaction favors preferentially the *gauche* conformer followed by the orbital interaction energy accounting for charge transfer effects. In the same study, [31] NBO indicates that stereoelectronic effects work in favor of *gauche* conformers.

Other more complex systems have been also computationally examined to analyze the conformational effects associated to the introduction of fluorine atoms. DFT geometry optimizations followed by MP2 single point calculations have revealed that the conformational landscape of a series of 25 benzyl alcohols is significantly influenced by the presence of one or two fluorine atoms in the *ortho* position.[32] Intramolecular interactions characterized in terms of Atoms in Molecules (AIM), Noncovalent Interactions (NCI) and NBO analyses, show that OH···F, CH···F and/or CH···O intramolecular contacts contribute to the stabilization of the various conformations.[32] On the other hand, the origin of the drastically different structure adopted by linear perfluoroalkanes and hydrocarbons (*i.e* helical vs zig-zag) has been inspected by means of NBO/NCI analyses using DFT wave functions. The energetic preference for the helical structures increases monotonically with the chain length of the perfluorated alkane, what has been explained in terms of $\sigma_{CC} \rightarrow \sigma_{CF}^{*}$ hyperconjugative interactions, which are absent in the zigzag conformation.[33]

1: 1,2-difluoroethane   **2:** 2-fluoroethyl-acetate   **3:** 3-fluoropropanal   **4:** *N*-(2-fluoroethyl)acetamide

5: 2-(2-fluoroethyl)isoindoline-1,3-dione   **6:** 2-fluoroethan-1-aminium   **7:** 1-(2-fluoroethyl)pyridin-1-ium

8: 1-fluoropropan-2-one   **9:** methyl-2-fluoroacetate   **10:** 2-fluoro-*N*-methylacetamide

11: 1,2,3-trifluoropropane   **12:** 2,3-difluoro-*N*-methyl propanamide   **13:** 2-(2,3-difluoropropyl) isoindoline-1,3-dione

14a/14b

Scheme 1

From our review of the former computational investigations, it turns out that a variety of effects may be behind the conformational preferences observed in fluorinated systems. However, direct comparisons among the results obtained in these studies are largely hampered by the diversity of methodologies employed. Therefore, we pursue in this work to reexamine the conformational effects exerted by fluorine atoms using a common methodology based on the IQA energy partitioning augmented with pairwise dispersion energies. The dispersion-corrected IQA approach facilitates the decomposition of the global conformational energies into fragment contributions that can be further separated into various quantum mechanical and classical electrostatic terms. To better appreciate the conformational impact of these energy contributions, we will consider two classes of organic

compounds. On one hand, we will evaluate intra and inter-atomic contributions to the relative energy of the *gauche*/*anti* conformers of fluoroethylene-derived systems (**1-7** in Scheme 1), the *trans*/*cis* conformers in carbonyl containing systems (**8-10**), and the combined *gauche-gauche* or *gauche-trans* preferences (**11-13**). On the other hand, we will characterize in detail the conformational properties of two diastereomers of an α,β-difluoro-γ-amino-acid derivative (**14a/14b** in Scheme 1) that have been proposed to be particularly relevant for the design of shape-controlled bioactive amino acids and peptides,[14] as they may link to other amino acids resulting in peptides with predictable conformational behavior. According to their crystal structures, the different stereochemistry at the α and β carbons, (*R,R*) for **14a** and (*R,S*) for **14b**, results in a different backbone conformation (extended zig-zag in **14a** and partially bent in **14b**). Both structures exhibit the normally expected *gauche* orientation in the F_{23}-C_{22}-C_{19}-F_{20} and F_{20}-C_{19}-C_{16}-N_{13} bonds and the antiparallel alignment (*trans*-planar) of the F_{23}-C_{22}-C_{25}=O_{26} moiety. In fact, these three effects are supposed to determine the final conformation of the **14a** and **14b** molecules. All in all, we report theoretical results obtained for typical model systems prone to characterize specific conformational effects, but also for actual fluorinated compounds of synthetic and biochemical interest. The IQA methodology will allow us to treat them on the same basis, yielding thus a full energetic description of the various effects influencing their conformational preferences.

Computational methods

IQA energy decomposition

The IQA approach[34] partitions the first- and second-order reduced density matrices into atomic regions such as the attraction basins (Ω_A) that stem from the topological properties of the charge distribution $\rho(r)$ as commonly defined within the framework of the quantum theory of atoms in molecules (QTAIM). Two scalar fields derived from quantum mechanical (QM) wavefunctions are required to accomplish the IQA decomposition: the first order reduced density matrix $\rho_1(\mathbf{r_1},\mathbf{r_1}')$ and the pair density, $\rho_2(\mathbf{r_1},\mathbf{r_2})$. Then IQA decomposes the total energy of a molecular system in the gas-phase as

$$E = \sum_A E_{net}^A + \sum_{A>B} E_{int}^{AB} = \sum_A \left(T^A + V_{ne}^{AA} + V_{ee}^{AA} \right) + \sum_{A>B} \left(V_{nn}^{AB} + V_{ne}^{AB} + V_{ne}^{BA} + V_{ee}^{AB} \right) \tag{1}$$

where $E_{net}^{A} \equiv E_{net}\left(\Omega_A\right)$ is the net electronic energy of atom A that includes the kinetic energy T^A and the potential energy due to nuclei-electron (*ne*) attractions and electron-electron repulsions (*ee*) within Ω_A. The interaction energy $E_{int}^{AB} = E_{int}\left(\Omega_A, \Omega_B\right)$ between atoms A and B in the molecular system collects various potential energy terms (*nn*, *en*, *ne* and *ee*). We stress that, according to the IQA terminology, an *interaction* energy is a diatomic contribution to the total energy of a molecule. In fact, the interaction energy E_{int}^{AB} can be divided into classical and non-classical contributions, allowing thus to define a purely classical (electrostatic) component of the interaction energy, $E_{int,class}^{AB} = V_{nn}^{AB} + V_{ne}^{AB} + V_{ne}^{BA} + V_{ee,Coul}^{AB}$, along with a quantum (exchange-correlation) contribution such that $E_{int}^{AB} = E_{int,class}^{AB} + E_{int,xc}^{AB}$. In this respect, we note also that the *classical* IQA components are distinguished only in the diatomic interaction terms E_{int}^{AB} , but not within the atomic net energies E_{net}^{A} .

By summing separately all the atomic and diatomic terms in equation (1), the total energy of a molecule is readily decomposed into net and interaction energy components (

$E_{net} = \sum_{A} E_{net}^{A},\ E_{int,class} = \sum_{A<B} \Delta E_{int,class}^{AB},...$). By inserting the corresponding IQA energies for a given

pair of *gauche* and *anti* conformers, the energy difference $E_{gauche}-E_{anti}$ can be written as

$$\Delta E = E^{gauche} - E^{anti} = \Delta E_{net} + \Delta E_{int,class} + \Delta E_{int,xc} \tag{2}$$

Dispersion corrected IQA

In previous work,[35] we have shown that IQA calculations can be complemented with the pairwise formulation of the third-generation dispersion (D3) correction for DFT and HF methods,[36] which is a semiclassical potential inspired on the London formula for the dispersion attraction between two atoms A and B at large distance and that does not alter the underlying charge density. The correct asymptotic behavior of the A-B dispersion energy can be reproduced using the Becke-Johnson (BJ)[37] rational damping function, resulting in the D3(BJ) dispersion energy correction (termed simply as D3 in the manuscript) that can be readily combined with the IQA decomposition scheme. To this end, we simply add the dispersion interaction energies $E_{int,disp}^{AB}$ to the rest of the IQA interaction energy terms such that the total D3-corrected IQA decomposition results,

$$E = \sum_A E_{net}^A + \sum_{A>B} \left(E_{int,class}^{AB} + E_{int,xc}^{AB} + E_{int,disp}^{AB} \right) \tag{3}$$

To keep the computational cost of the IQA calculations withtin reasonable bounds, all the IQA-D3 calculations are done with HF wavefunctions. In fact HF-D3 method provides a reasonable description of molecular structure and energetics,[38, 39] and offers a straightforward physical partitioning because HF entirely lacks dispersion energy. To further assess the utility of the HF-D3 IQA decomposition, we briefly compare in the Supporting Information (Table S12) the HF-D3 IQA results on 1,2-difluoethane with those obtained with correlated methods (B3LYP-D3 and MP2).

Interacting Quantum Fragments (IQF-D3)

In principle, the grouping of the atomic IQA energy components into chemically-meaningful fragment contributions can be done using different notations and protocols depending on the particular problem at hand. For example, to characterize the conformational energy variation upon an internal rotation about a single bond, we will distinguish at least two molecular fragments, P and Q, that are covalently linked (P-Q) through the rotating bond. Such interacting quantum fragments (IQF) partitioning of a molecular system splits the total energy in intra-fragment and inter-fragment energy terms. The intra-fragment net energy (E_{net}^P and E_{net}^Q) collects the atomic net energies and the interaction energies among the atoms placed in the same fragment, whereas the inter-fragment term (E_{int}^{PQ}) sums the classical and quantum interaction energies between atoms in different groups.

Using IQF-D3 quantities, the relative energy ΔE between the *gauche* and *anti* conformers around the P-Q bond can be expressed as:

$$\Delta E = \Delta E_{net}^P + \Delta E_{net}^Q + \Delta E_{int,class}^{PQ} + \Delta E_{int,xc}^{PQ} + \Delta E_{int,disp}^{PQ} \tag{4}$$

where the relative IQF terms in the right hand are just the corresponding *gauche/anti* differences of the grouped terms ($e.g, \Delta E_{net}^P = E_{net}^{P,\text{gauche}} - E_{net}^{P,anti}$) and the ΔE_{int}^{PQ} term is split into the classical interaction energy $\Delta E_{int,class}^{PQ}$ and the purely QM correlation-exchange contribution $\Delta E_{int,xc}^{PQ}$.

To further clarify the meaning of the IQF terms, it may be useful to briefly discuss the similarities and differences between IQF and the energy decomposition analysis (EDA).[40, 41]

Assuming that EDA is applied to analyze the energy difference between two conformers of the *P-Q* system with reference to separated (unrelaxed) $P\cdot$ and $Q\cdot$ radical fragments, ΔE would be the sum of three terms: a classical electrostatic interaction energy between $P\cdot$ and $Q\cdot$ (V_{elstat}), a Pauli repulsion term (ΔE_{Pauli}) that incorporates the kinetic and potential energy changes due to the antisymmetrization of the fragment wavefunctions, and an orbital relaxation energy (ΔE_{orb}) that arises from inter-fragment charge transfer and polarization effects. In general, the $\Delta E_{net}^{P} + \Delta E_{net}^{Q} + \Delta E_{int,xc}^{PQ}$ sum in IQF (termed as exchange-correlation-repulsion) resembles the $\Delta E_{Pauli} + \Delta E_{orb}$ sum in EDA, while $\Delta E_{int,class}^{PQ}$ would correspond to V_{elstat} although this identification is exact only in the limit of weakly interacting fragments for which ΔE_{orb} tends to zero.[42] Nevertheless, the grouped EDA and IQF terms admit a similar interpretation on the basis of electrostatic and/or QM effects. However, the IQF balance between intra-fragment deformation ($\Delta E_{net}^{P} + \Delta E_{net}^{Q}$) and inter-fragment exchange-correlation effects ($\Delta E_{int,xc}^{PQ}$) provides an alternative description of the QM effects embedded in the $\Delta E_{Pauli} + \Delta E_{orb}$ term without referring to separate fragments.

Charge and Dipole electrostatic interactions

In order to deepen the description of the IQF $\Delta E_{int,class}^{PQ}$ term, the multipole expansion of the electrostatic potential may be useful for assessing the role of the charge distribution in the *P* and *Q* regions. In fact the QTAIM and IQA approaches allow us to express the Coulombic energy as a multicenter multipole expansion in a natural way.[43] It is well known that the electrostatic potential exerted by a set of point charges at a sufficiently distant point can be expanded in terms of multipole moments. In our study we focus on the first two contributions to the electrostatic potential, *i.e.*, the total charge of a given basin (*q*) and the dipole moment (*d*) emerged from its distribution. Hence, only the charge-charge, charge-dipole and dipole-dipole interactions have been considered. Their respective analytical formulation are given in Eqs. (5)-(7) (in atomic units):

$$E_{qq} = \frac{q^{P} q^{Q}}{R} \tag{5}$$

$$E_{qd} = \frac{q^{P} \mu^{Q} \mathbf{R}}{R^{3}} \tag{6}$$

$$E_{dd} = \frac{R^2 \boldsymbol{\mu}^P \boldsymbol{\mu}^Q - 3(\boldsymbol{\mu}^P \mathbf{R})(\boldsymbol{\mu}^Q \mathbf{R})}{R^5} \qquad (7)$$

where the superscripts P and Q denote the two fragments considered, $\mathbf{R}$ represents the distance between their centers of mass, q^P / q^Q are the total charge in P/Q (*i.e.*, $q^P = \sum_{A \in P} q^A$) and $\boldsymbol{\mu}^P/\boldsymbol{\mu}^Q$ are the dipole moment generated by the total charge distribution within P/Q.

Starting from the atomic dipoles arisen upon a particular 3D partitioning of the space, it is not, in general, straightforward to reconstruct fragment dipoles from atomic ones. The simple addition of the corresponding dipole components is not sufficient for the study of the charge-dipole or dipole-dipole fragment interactions. For neutral molecules but not for ions, $\boldsymbol{\mu}$ is origin independent since any coordinate transformation $\mathbf{r} = \mathbf{r}' + \mathbf{R}_0$ gives

$$\boldsymbol{\mu} = \int \mathbf{r}\rho(\mathbf{r}) d\mathbf{r} = \int \mathbf{r}'\rho(\mathbf{r}' + \mathbf{R}_0) d\mathbf{r}' + \mathbf{R}_0 \int \rho(\mathbf{r}' + \mathbf{R}_0) d\mathbf{r}' = \int \mathbf{r}'\rho(\mathbf{r}' + \mathbf{R}_0) d\mathbf{r}' + \mathbf{R}_0 q \qquad (8)$$

so that the charge-translation $\mathbf{R}_0 q$ term vanishes for neutral molecules. To derive an atomic decomposition of $\boldsymbol{\mu}$, the charge density ρ can be partitioned into disjoint atomic regions with their own origin of coordinates at positions $\mathbf{R}_0^A$, and performing thus a transformation $\mathbf{r} = \mathbf{r}^A + \mathbf{R}_0^A$ in each basin. The total dipole is then expressed as

$$\boldsymbol{\mu} = \sum_A \left(\int_{\Omega_A} \mathbf{r}^A \rho(\mathbf{r}^A + \mathbf{R}_0^A) d\mathbf{r}^A + \mathbf{R}_0^A \int_{\Omega_A} \rho(\mathbf{r}^A + \mathbf{R}_0^A) d\mathbf{r}^A \right) = \sum_A \left(\boldsymbol{\mu}_{int}^A + \mathbf{R}_0^A q^A \right) \qquad (9)$$

Eq. (9) shows that $\boldsymbol{\mu}$ is the summation of atomic dipoles $\boldsymbol{\mu}^A$ that have two contributions: the *intrinsic* term $\boldsymbol{\mu}_{int}^A$ that comes from the integration of the dipole density function within the atomic basin plus the corresponding charge-translation term $\mathbf{R}_0^A q^A$. Fragment-based dipoles $\boldsymbol{\mu}^P$ can be likewise defined by considering both the intrinsic contributions and the net charges q^A of the atomic basins that constitute fragment P:

$$\boldsymbol{\mu}^P = \sum_{A \in P} \boldsymbol{\mu}_{int}^A + \sum_{A \in P} \left(\mathbf{R}_0^A - \mathbf{R}_0^P \right) q^A \qquad (10)$$

The reconstructed dipoles $\boldsymbol{\mu}^P$ depend on the origin of coordinates which, in this work, are selected as the center of mass of fragment P ($\mathbf{R}_0^P$). We note that, in the case of neutral molecules, the dependency of the $\boldsymbol{\mu}^P$ values on the origin of coordinates is small. We also

emphasize that the total electrostatic interaction energy among the various atoms/fragments in a given molecule computed from the multipolar expansion is always origin-independent.

QM calculations

Initial coordinates for the small and medium-sized models were generated using the UCSF Chimera program.[44] Starting from 1,2-difluoroethane in the *gauche* conformation, all the CH_2F-CH_2X systems were built in the *gauche* conformation by replacing the second fluorine atom by the appropriate X group. Then the initial geometries of the corresponding *anti* conformers were obtained by adjusting the F-C-C-X angle to 180º. Similarly, we built the initial *trans/cis* conformers for the CH_2F-COX systems.

All the *gauche/anti* and *trans/cis* structures of the small models were fully optimized in the gas-phase with no symmetry constraints at the HF-D3/cc-pVTZ and the RI-MP2/cc-pVTZ levels of theory. These calculations were done with the ORCA 4.0.1 package.[45] The HF-D3/cc-pVTZ energy minimizations were carried out with the D3 dispersion energy and gradient corrections choosing the Becke-Johnson (BJ) damping function.[36, 37] The resolution-of-the-identity (RI) approximation was activated for the MP2 calculations using the appropriate auxiliary basis set. To further estimate electron correlation effects on the conformational energies, we employed the domain-based Local Pair Natural Orbital (DLPNO) coupled cluster method[45, 46] as implemented in the ORCA 4.0.1 package. More specifically, we performed DLPNO-CCSD(T)/aug-cc-pVTZ single point calculations on the MP2/cc-pVTZ geometries using tight thresholds to control the DLPNO approximations. The DLPNO-CCSD(T) method exhibits near linear scaling at the cost of introducing small deviations from the canonical coupled cluster methods. For tight DLPNO thresholds, the typical errors with respect to canonical results are below 0.25 kcal/mol.[47]

For 1,2,3-trifluoropropane and the related CH_2F-CHF-CH_2X system with an isoindole-derivative as the X substituent, initial coordinates were generated by setting the F-C-C-F and F-C-C-X angles to ±60º and/or 180º, resulting in nine structures accordingly named *g+/g+*, *g+/g-, g+/anti*, etc. In the case of the CH_2F-CHF-$CONHCH_3$ molecule, the F-C-C=O angle takes the values 180º for the *trans* and 0º for the *cis* conformers, which combined with the three options available for the F-C-C-F torsion result in six initial structures termed *g+/trans, g+/cis, g-/trans*, etc. As in the smaller CH_2F-CH_2X systems, initial geometries were fully optimized in the gas-phase at the HF-D3/cc-pVTZ and the RI-MP2/cc-pVTZ levels of theory

followed by single point DLPNO-CCSD(T)/aug-cc-pVTZ calculations on the MP2/cc-pVTZ geometries.

For the **14a** and **14b** compounds, automatic conformational analyses were performed using the multiconformer generator MS-DOCK program.[48] Starting from the corresponding crystal structures,[14] we used the antechamber program to optimize the initial geometries and to assign AM1-BCC atomic charges and SYBYL atom types.[49] Subsequently, 50 different conformers were generated for **14a** and **14b** using the MS-DOCK software and the resulting structures were optimized using the MMFF94 force field. During conformer generation, a filter based on the root mean squared deviation of the Cartesian coordinates and the energy was applied to eliminate similar structures. The **14a** and **14b** different conformers were then optimized at the HF-D3/cc-pVDZ level of theory using the ORCA 4.0.1 program.[45] After inspection of the structure and energy of the minimized structures, only 20 different conformers remained for **14a** and **14b**. These were reoptimized at the HF-D3/cc-pVTZ level of theory using ORCA both in the gas phase and in chloroform using the SMD continuum solvent model.[50] For the five more stable conformers of **14a** and **14b**, selected NMR vicinal proton-fluorine coupling constants $^3J_{H,F}$ were estimated using a seven-parameter Karplus-type relation.[51] The equation correlates a $^3J_{H,F}$ value with the corresponding H-C-C-F torsion angle and it also includes correction terms for substituent electronegativity a well as for H-C-C and F-C-C bonds angles. The $^3J_{H,F}$ values were computed using the HF geometries optimized in chloroform, whereas the electronegativity values for the Cα-Cβ substituents (1.4 for fluorine, 0.9 for carbon and 0.0 for hydrogen) were taken from reference 51.

Promolden calculations

The IQA decomposition of molecular energies at the HF-D3/cc-pVTZ level was performed with a modular version of the PROMOLDEN program[52] that is being developed in our laboratory. As previously noticed, the pairwise dispersion energies computed with the DFTD3 program[53] are combined with the various IQA terms ($E_{\mathrm{net}}\left(\Omega_A\right)$, $E_{\mathrm{int}}\left(\Omega_A,\Omega_B\right)$, …) to formulate the IQA-D3 energy decomposition of the corresponding HF-D3 energies (*i.e.*, three-body dipole–dipole–dipole dispersion energy is not included). The IQA quantities are numerically integrated over the atomic basins Ω_A, which constitute finite and irregular integration domains, using very large angular and radial grids in atomic spherical quadratures. We adopted integration settings that represent a compromise choice between computational cost and accuracy for small and medium-sized molecules. Thus, a β–sphere around each atom

12

was considered (*i.e.*, a sphere completely contained inside the atomic basin), with a radius equal to 60 % the distance of its nucleus to the closest bond critical point in the electron density. High-quality Lebedev angular grids were used with 5810 and 974 points outside and within the β-spheres of heavy atoms, respectively, (3890 and 590 points for hydrogen atoms). Euler-McLaurin radial quadratures were employed with 512 and 384 radial points outside and inside the β–spheres of heavy atoms, respectively (384 and 256 points for H). The largest value of the radial coordinate in the integrations was 15.0 au for heavy atoms (10.0 au for H atoms). Maximum angular moments, λ_{max}, of 10 and 6 were assigned to the Laplace and bipolar expansions of the $1/r_{12}$ operator outside and within the β-spheres.

Most of the IQA calculations reported in this work were computed with the conventional $\mathcal{O}(N^4)$ algorithm implemented in PROMOLDEN that employs the N occupied canonical molecular orbitals (MO) to expand the first and second-order density matrices. For the **14a/14b** compounds that have 51 atoms, the $\mathcal{O}(N^4)$ algorithm is exceedingly expensive and, therefore, we used a variant that uses localized MOs and employs the multipolar approach[54] for computing selected interatomic exchange-correlation (xc) energies. The LMOs were computed with the Pipek-Mezey algorithm[55] as implemented in the ORCA 4.0.1 package. For each atomic basin Ω_A, a subset of LMOs $\left\{\phi_i^{LMO}\right\}_A$ is then built by requiring that their diagonal contribution to the atomic overlap matrix ($\int_{\Omega_A} \left|\phi_i^{LMO}\right|^2 d\tau$) is greater than 10^{-6} au. The calculation of the IQA $E_{net}(\Omega_A)$ terms are done using the corresponding subset $\left\{\phi_i^{LMO}\right\}_A$ for each basin. For the calculation of the diatomic $E_{int}(\Omega_A, \Omega_B)$ terms, the LMO sets of the pair of basins are combined as the union $\left\{\phi_i^{LMO}\right\}_A \cup \left\{\phi_j^{LMO}\right\}_B$ or intersection $\left\{\phi_i^{LMO}\right\}_A \cap \left\{\phi_j^{LMO}\right\}_B$ in order to integrate the Coulombic or exchange-correlation interactions, respectively. The multipolar *xc* approximation at high order of the angular momentum series ($L=10$) is activated for 1-*n* (*n*>4) intramolecular interactions provided that the interatomic R_{AB} distance is greater than 5.0 au. For $R_{AB} >17$ au, the $E_{int}^{xc}(\Omega_A, \Omega_B)$ values are neglected. The goodness of these additional approximations was tested by comparing the results of conventional (MO-based) and LMO-based IQA calculations on the conformers of 2,3-difluoro-*N*-methylpropanamide and 2-(2,3-difluoropropyl)isoindoline-1,3-dione (**12** and **13** in Scheme 1). The IQA error defined as $\left|E - E^{IQA}\right|$, where E is the total energy obtained from the QM calculations and E^{IQA} is the total
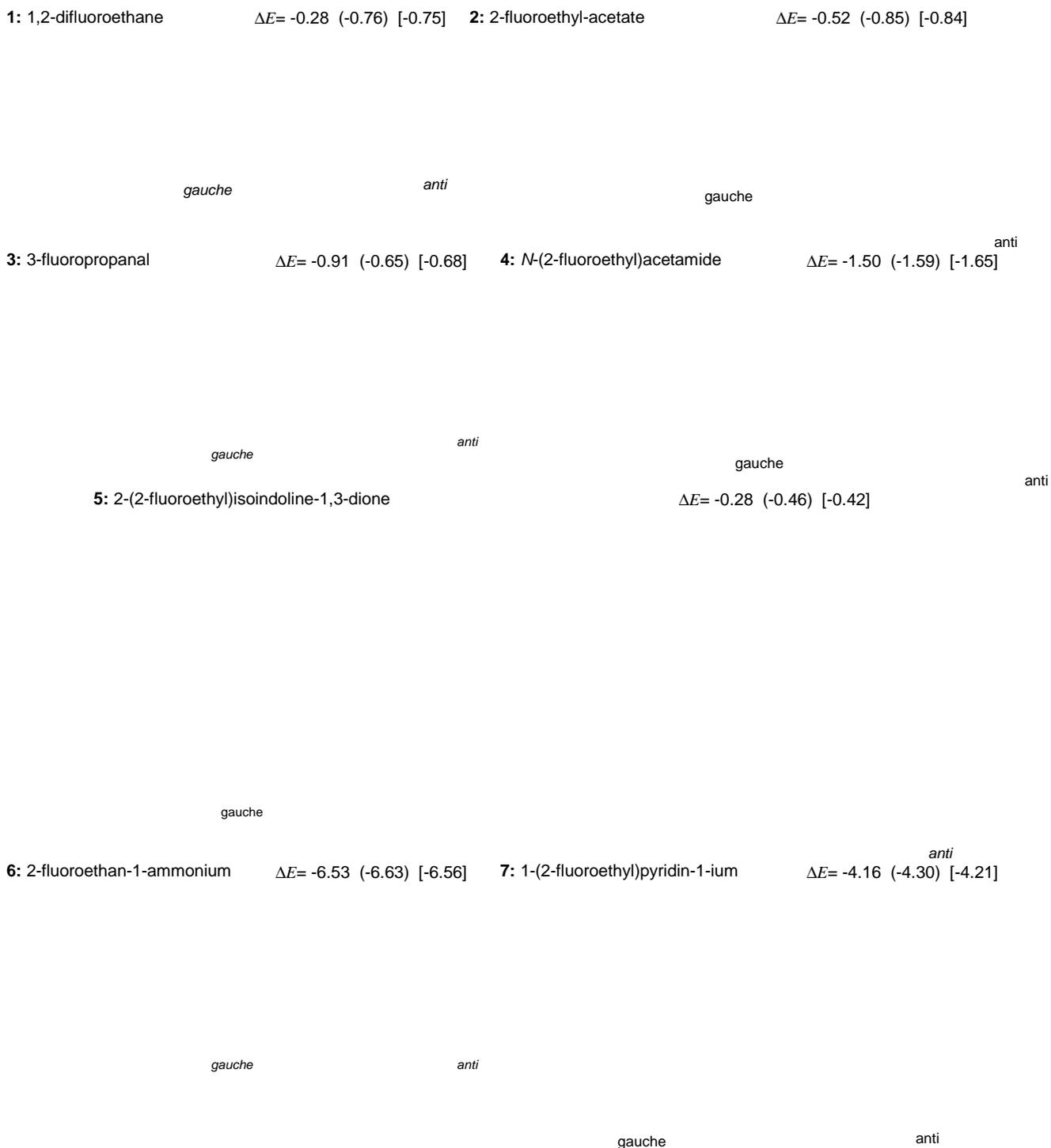
energy reconstructed from the IQA terms, had average values of 0.5 kcal/mol (**12**) and 0.9 kcal/mol (**13**) for the MO-based IQA calculations. The corresponding values for the LMO/multipolar-based IQA calculations were similar: 0.5 kcal/mol (**12**) and 1.2 kcal/mol (**13**). Hence, the additional numerical error due to the LMO and multipolar approximations is expected to be small without compromising the conclusions of the IQA analysis.

Results

As above mentioned, 1,2-difluoroethane is usually considered as the reference system to analyze the *gauche*/*anti* conformational preference associated to adjacent fluorine atoms. For this reason, initial models for the *gauche* (F-C-C-F 60º) and *anti* (F-C-C-F 180º) conformers of 1,2-difluoroethane were optimized in the gas phase at the HF-D3/cc-pVTZ and MP2/cc-pVTZ levels of theory. Both geometry optimizations provided very similar structures, with the largest differences in the geometries located in the C-F bond lengths (see Figure 1). Relative energies were further reevaluated by means of DLPNO-CCSD(T)/aug-cc-pVTZ single point calculations performed on the MP2 geometries (see Figure 1), the *gauche* conformer being 0.7 kcal/mol more stable than the *anti* one in agreement with previous results (unless otherwise noticed ΔE values in the text correspond to DLPNO-CCSD(T) data).

Clearly, the magnitude of the *gauche* effect in 1,2-difluoroethane seems too scarce to allow the design of molecules with a frozen conformation. Hence, it is interesting to examine how the *gauche* preference can be modulated in other systems. Actually, replacing one of the fluorine atoms in 1,2-difluoroethane for other functional groups could drive away the energy of the *gauche* and *anti* conformers, increasing the impact of a single C-F bond in selecting a particular conformation. To further clarify this point, we optimized the *gauche* and *anti* conformers for a number of β-substituted α-fluoroethanes (see **1-7** in Scheme1 and Figure 1). Among the neutral molecules in Figure 1, the largest *gauche*/*anti* conformational preference is achieved for acetamide with 1.6 kcal/mol favoring the *gauche* conformation. A more pronounced *gauche* preference is induced by a positive charge adjacent to the fluorine atom. Thus, *gauche* structures with either ammonium or pyridinium groups are 6.6 and 4.2 kcal/mol, respectively, more stable than the corresponding *anti* ones.

Figure 1. Ball-and-stick representation of the gauche/anti conformers optimized for different CH_2F-CH_2-X systems. The C-F and C-C bond distances (Å), the F-C-C-X dihedral angle (º), and selected intramolecular distances (Å) measured in the HF-D3/cc-pVTZ optimized structures (RI-MP2/cc-pVTZ in parentheses) are shown. Energy differences ($E_{gauche}-E_{anti}$) in kcal/mol computed at the HF-D3/cc-pVTZ, RI-MP2/cc-pVTZ (in parentheses) and DLPNO-CCSD(T)/aug-cc-pVTZ [in brackets] levels of theory are also included.

1: 1,2-difluoroethane ΔE= -0.28 (-0.76) [-0.75]   **2:** 2-fluoroethyl-acetate ΔE= -0.52 (-0.85) [-0.84]

gauche   *anti*   gauche

                                                                              anti

3: 3-fluoropropanal ΔE= -0.91 (-0.65) [-0.68]   **4:** *N*-(2-fluoroethyl)acetamide ΔE= -1.50 (-1.59) [-1.65]

gauche   *anti*   gauche

                                                                              anti

5: 2-(2-fluoroethyl)isoindoline-1,3-dione ΔE= -0.28 (-0.46) [-0.42]

gauche

6: 2-fluoroethan-1-ammonium ΔE= -6.53 (-6.63) [-6.56]   **7:** 1-(2-fluoroethyl)pyridin-1-ium ΔE= -4.16 (-4.30) [-4.21]

gauche   *anti*   *anti*

                              gauche   anti

When a carbonyl group is placed adjacent to a C-F bond as in α-fluoroamides, the *trans*-planar arrangement of the F-C-C=O moiety is energetically favored over the *cis* one. This is observed in Figure 2 for a ketone (**8**) and for an amide (**10**). In contrast, we computed an almost negligible *cis/trans* conformational preference for the ester (**9**).

Figure 2. Ball-and-stick representation of the *cis/trans* conformers optimized for different CH_2F-CO-X systems. The C-F and C-C distances (Å), the F-C-C=O dihedral angle (°) and selected intramolecular distances (Å) measured in the HF-D3/cc-pVTZ optimized structures (RI-MP2/cc-pVTZ in parentheses) are shown. Energy differences ($E_{trans}–E_{cis}$) in kcal/mol computed at the HF-D3/cc-pVTZ, RI-MP2/cc-pVTZ (in parentheses) and DLPNO-CCSD(T)/aug-cc-pVTZ (in squared brackets) levels of theory are also included.

8: 1-fluoropropan-2-one ΔE= -2.79 (-2.06) [-2.09]

cis   *trans*

9: methyl-2-fluoroacetate ΔE= -0.09 (0.04) [0.11]

cis

trans

10: 2-fluoro-*N*-methylacetamide ΔE= 5.80 (5.81) [5.64]

cis

trans

cis   *trans*

To analyze the origin of these energetic preferences, we carried out the IQA partitioning of the conformational energy differences at the HF-D3/cc-pVTZ level. In this respect, we note that relative energies in Figures 1 and 2 confirm that the HF-D3 ΔE values remain reasonably close to the DLPNO-CCSD(T) ones, the mean unsigned difference between them being 0.2 kcal/mol. Hence, we believe that this favorable comparison validates the use of the HF-D3 method in the subsequent IQA analyses.

Atomic and fragment-based IQA analysis of gauche/anti CH₂F-CH₂F

As described in Methods, IQA[56] decomposes molecular energy differences into a collection of atomic and interatomic terms. For 1,2-difluoroethane, the combination of the IQA quantities including the small dispersion contribution, results in an IQA reconstructed $\Delta E = E_{gauche} - E_{anti}$ energy difference of −0.5 kcal/mol, which is close to the HF-D3/cc-pVTZ reference value (−0.3 kcal/mol). This discrepancy is due to the numerical errors accumulated during the calculation of the IQA quantities. As the individual IQA terms are typically one or two orders of magnitude larger than ΔE, their expected relative error would be small.

Inspection of the IQA energies shows that the largest differences between the *gauche* and *anti* conformers arise in the electrostatic interactions (see Table S2). Thus, the *gauche* conformation is largely favored by the $\Delta E_{int,class}$ term corresponding to the $C_1 \cdots F_6$ (-8.0 kcal/mol) and $F_2 \cdots C_5$ (-7.9 kcal/mol) electrostatic contacts. However, this *gauche* stabilization is widely compensated by the repulsive $F_2 \cdots F_6$ (12.1 kcal/mol) and $C_1 \cdots C_5$ (6.9 kcal/mol) electrostatic terms. Moreover, the overall *gauche* preference is also affected by other atomic and diatomic IQA terms, as the $C_1 \cdots C_5$ exchange-correlation interaction (-3.2 kcal/mol), the F_2, F_6, and C_1 electronic distortions (ΔE_{net} = 1.1, 1.0 and 1.0 kcal/mol, respectively), etc. By summing over all the atomic and diatomic contributions (see Table S1), it arises that both the classical electrostatic ($\Delta E_{int,class}$=−2.3 kcal/mol) and the exchange-correlation ($\Delta E_{int,xc}$=−1.9 kcal/mol) interactions favor the *gauche* conformation in 1,2-difluoroethane.

By considering the 1,2-difluoroethane molecule as formed by two interacting quantum fragments (IQF), the *gauche*/*anti* conformational energy difference can be split into intra-fragment deformation terms and electrostatic and quantum-mechanical inter-fragment contributions. Due to the symmetric character of the two CH₂F groups, there is no net charge transfer between them so that ΔE_{net}^{P} and ΔE_{net}^{Q} collect the energetic impact of electronic reorganization within P and Q and of a minimal steric hindrance. The computed net energy differences for each CH₂F group are 0.6 and 0.4 kcal/mol (these distinct values are again due to IQA numerical errors), but the overall deformation (1.0 kcal/mol) favoring the *anti* orientation is clearly smaller than the inter-fragment energy changes (see Table 1). Thus, the largest contribution to the stabilization of the *gauche* conformer comes from the non-classical exchange-correlation interaction (-3.5 kcal/mol) between the CH₂F groups. In contrast, classical electrostatic effects clearly stabilize the *anti* conformer (2.1 kcal/mol), which is usually explained in terms of the repulsion arising from the nearly aligned C-F dipole moments

in the *gauche* orientation (*i.e.,* F-C-C-F dihedral ~60º). This interpretation seems partly correct because, according to our analyses, the dipole-dipole interaction accounts for 55% of the difference in the $CH_2F \cdots CH_2F$ electrostatic interaction between the *gauche/anti* conformers so that higher-order multipolar contributions would also be important. Anyway, it is the $\Delta E_{int,xc}^{PQ} + \Delta E_{int,class}^{PQ}$ sum (-1.4 kcal/mol) that mainly controls the stability of the gauche conformer and, therefore, the IQF energy decomposition for 1,2-difluoroethane resembles those in previous proposals about the combined role of hyperconjugation and electrostatics to explain the *gauche* effect.[23] Within the context of IQF, we propose then to measure the *gauche* stabilization in 1,2-difluoroethane and related systems as $\Delta E_{int,xc}^{PQ} + \Delta E_{int,class}^{PQ}$.

Probably, either the IQA or the IQF analysis of the *gauche/anti* 1,2-difluoroethane may be adequate and useful. Nonetheless, chemists usually explain molecular properties in terms of the functional groups or the characteristic moieties that build up a molecule. For large systems, grouping the atomic terms into fragments simplifies the interpretation of the IQA data because the IQF terms smooth out the correlated fluctuations of the atomic quantities within a given group. Therefore, we decided to focus on the IQF results for the rest of the systems studied in this work, although the underlying atomic partitioning will also be used to better characterize some relevant inter- or intra-fragment contributions.

Table 1. IQF energy components at the HF-D3/cc-pVTZ level for the energy difference (kcal/mol) between the two conformers (*gauche/anti* or *cis/trans*) analyzed for a series of small systems related to 1,2-difluoroethane. Two-fragment partitioning scheme ($P=CH_2F$ and $Q=CH_2X$) is assumed for the different systems.

$\Delta E = E_{gauche} - E_{anti}$	Δq^P	ΔE_{net}^P	ΔE_{net}^Q	$\Delta E_{int,disp}$	$\Delta E_{int,xc}$	$\Delta E_{int,class}$	$\Delta E_{int,class,qq}$	$\Delta E_{int,class,qd}$		$\Delta E_{int,class,dd}$	ΔE_{IQA}
1: 1,2-difluoroethane	0.00	0.6	0.4	-0.0	-3.5	2.1	0.0	0.0		1.1	-0.5
2: 2-fluoroethyl-acetate	0.00	0.7	0.5	-0.0	-3.1	1.4	0.0	0.0	0.0	-0.7	-0.5
3: 3-fluoropropanal	-0.01	0.0	1.4	-0.0	-1.1	-1.5	-0.1	-0.4	0.0	-0.4	-1.2
4: *N*-(2-fluoroethyl)acetamide	-0.02	-0.6	2.1	-0.2	-2.1	-1.4	-0.2	-0.6	0.1	-1.0	-2.1
5: 2-(2-fluoroethyl)isoindoline-1,3-dione	0.00	2.0	1.5	-0.3	-3.6	-0.1	0.0	-0.0	-0.0	0.1	-0.5
6: 2-fluoroethxan-1-aminium	-0.01	1.6	4.7	-0.6	-6.9	-6.0	2.4	1.3	-3.5	-4.6	-7.3
7: 1-(2-fluoroethyl)pyridin-1-ium	-0.01	1.0	3.5	-0.3	-5.5	-3.7	0.9	0.2	-6.1	-0.3	-5.1
$\Delta E = E_{trans} - E_{cis}$	Δq^P	ΔE_{net}^P	ΔE_{net}^Q	$\Delta E_{int,disp}$	$\Delta E_{int,xc}$	$\Delta E_{int,class}$	$\Delta E_{int,class,qq}$	$\Delta E_{int,class,qd}$		$\Delta E_{int,class,dd}$	ΔE_{IQA}
8: 1-fluoropropan-2-one	0.01	0.1	0.6	0.0	1.5	-4.9	0.0	-0.1	0.1	-2.9	-2.8
9: methyl-2-fluoroacetate	0.00	0.6	0.5	0.0	0.3	-1.4	0.0	0.7	0.2	-2.8	-0.1
10: 2-fluoro-N-methylacetamide	-0.02	2.1	2.7	-0.2	-4.1	-6.3	0.0	0.2	0.1	-5.2	-5.8

Substituent effects on the gauche/anti CH₂F-CH₂X conformers: Competition between IQF exchange-correlation and electrostatic interactions

For the CH_2F-CH_2X molecules, the *gauche* conformer is energetically favored over the *anti* one (see Figure 1). In all the CH_2F-CH_2X molecules, the charge variation at the CH_2F / CH_2X moieties upon the *anti→gauche* rearrangement is null or minimal (~0.01 e) as computed from the corresponding QTAIM charges.

Regarding 1,2-difluoroethane as the reference compound, we observe that replacing the second fluorine atom by an acetate group (**2** in Scheme 1) results in very small changes in the IQF terms. Again the *gauche* conformer is stabilized by the exchange correlation interaction ($\Delta E_{int,xc}$=−3.1 kcal/mol). Electrostatics favors the *anti* geometry ($\Delta E_{int,class}$=1.4 kcal/mol), but such effect does not arise from favorable μ-μ interactions ($\Delta E_{int,class,dd}$=−0.7 kcal/mol). This is due to the internal geometry of the acetate group, in which the dipole moments along the C=O/C-O bonds combine in a total fragment dipole moment (~1.9 D) that is nearly orthogonal to the CH_2F dipole (~2.2 D) in the *anti* conformer.

Introduction of an aldehyde (**3**) or an amide (**4**) group leads to classical and exchange-correlation inter-fragment interactions that stabilize the *gauche* conformer, being partially compensated by the unfavorable net energy change of the CH_2X fragment (see Table 1). There are, however, some differences between the aldehyde and the amide groups. The largest inter-atomic electrostatic interaction involves the fluorine atom in the two systems, but the F_2···C_8 interaction in the aldehyde **3** stabilizes the *gauche* structure (-15.9 kcal/mol), meanwhile the equivalent F_2···N_6 contact stabilizes the *anti* conformation in **4** (27.9 kcal/mol). If we compare the electrostatic F_2···N_6 interaction in the amide with F_2···O_6 in **2** (20.8 kcal/mol) and F_2···F_6 in **1** (12.1 kcal/mol), it arises an inverse relationship between the electronegativity of the X atom in the F-C-C-X sequence and the penalty for the *gauche* orientation due to the F···X $\Delta E_{int,class}$ electrostatic term.

In contrast with the **1-4** systems, the small *gauche* stabilization computed for the isoindole derivative **5** arises from a large and favorable exchange-correlation term (-3.6 kcal/mol), mainly ascribed to the H_3···O_{19} and F_2···N_{20} interactions (see Table S2). But this favorable $\Delta E_{int,xc}$ term is cancelled by the intra-fragment net energies (2.0 and 1.5 kcal/mol). The change in the inter-fragment electrostatic interaction is almost negligible (-0.1 kcal/mol) due to the cancelation of large inter-atomic electrostatic interactions between fluorine and the heteroatoms in the isoindole moiety.

19

A cationic group adjacent to a C-F bond significantly stabilizes the *gauche* conformation, what is commonly explained in terms electrostatics. In effect, the $\Delta E_{int,class}$ terms in the *gauche–anti* energy difference in $CH_2F\text{-}CH_2X^+$ become quite important: -6.0 and -3.7 kcal/mol for the ammonium (**6**) and pyridinium (**7**) groups. These two cationic substituents have different size and charge distribution, what is reflected in their μ^Q dipole moments, ~2.5 D and ~0.2/0.5 D for the ammonium and pyridinium CH_2X^+ groups, respectively. The global positive charge is delocalized between the *P* and *Q* fragments (*e.g.*, q^P=0.12 and q^Q= 0.88 in the gauche **6** conformer) and these q^P/ q^Q charges repel more strongly in the *gauche* orientation. Thus, the charge-dipole and dipole-dipole fragment interactions explain the electrostatic preference for the *gauche* location of the ammonium group (see Table 1), while the rather small μ^Q value of pyridinum implies that only the interaction between the bulkier pyridinium charge and the CH_2F dipole makes a relevant contribution to the *gauche* stability (-6.1 kcal/mol). As in the $CH_2F\text{-}CH_2X$ neutral systems, the change in the fragment net energies stabilizes the *anti* orientation in the cationic systems albeit with a more pronounced influence (*e.g.*, ΔE_{net}^Q =4.7 and 3.5 kcal/mol for **6** and **7**). However, the IQF data reveals that the exchange-correlation inter-fragment interactions reinforce the stability of the *gauche* orientation (see Table 1) and compensate the deformation energies. More particularly, in the *gauche* **6** structure, a short F···H-N contact rationalizes well the significant $\Delta E_{int,xc}^{PQ}$ value of -6.9 kcal/mol (see Table S2 and Figure 1).

IQF description of trans/cis conformers in $CH_2F\text{-}(C=O)X$: Electrostatic control

When a carbonyl group is placed adjacent to a fluorine atom, electrostatic effects are assumed to stabilize the *trans*-planar orientation of the C=O and C-F groups over the *cis* one (see Figure 2). Our IQF calculations on the α-fluoroketone (**8**), α-fluoroester (**9**), and α-fluoroamide (**10**) molecules confirm that the electrostatic interaction between the CH_2F and (C=O)X moieties is the key element that explains the larger stability of the C-F/C=O *trans* arrangement ($\Delta E_{int,class}$ = -4.9, -1.4 and -6.2 kcal/mol for **8**, **9** and **10**; see Table 1). Furthermore, this electrostatic effect is mainly associated to the dipole-dipole interaction term in the three cases, although contributions from higher multipoles seem also relevant for the α-fluoroketone **8**. The exchange-correlation term also contributes to the stability of the *trans* fluoroamide (-4.1 kcal/mol), whereas it favors the *cis* orientation in the fluoroketone (1.5

kcal/mol) and has little effect on the α-fluoroester. These $\Delta E_{int,xc}$ contributions mainly result from the $F_2 \cdots O_6$ (4.5 kcal/mol)/$F_2 \cdots C_7$ (-3.1) interactions in the *cis/trans* α-fluoroketone **8**, and the $F_2 \cdots N_7$ (-5.3)/$F_2 \cdots O_6$ (4.7)/$F_2 \cdots H_8$ (-3.0) contacts in the α-fluoroamide **10**. Nonetheless, the favorable F$\cdots$H-N polar contact in **10** is nearly compensated by significant fragment distortion (see ΔE_{net}^{P} and ΔE_{net}^{Q} in Table 1) so that the electrostatic $\Delta E_{int,class}$ is the major stabilizing energy contribution to the *trans* preference between the vicinal C-F and C=O groups.

–CF–CF–CF– motif: IQA discrimination among gauche effects, 1,3 dipole-dipole and 1,3 CH$\cdots$F contacts

For large molecules bearing various fluorine atoms as well as other functional groups, several fluorine-associated effects may control their conformational preferences. For instance, the preferred conformations in polyfluorinated alkanes have been assumed to arise from maximizing *gauche* interactions between vicinal fluorine atoms and, simultaneously, minimizing unfavorable dipole-dipole interactions between 1,3-difluoro motifs.[9, 13] To further analyze these effects, we optimized the nine conformers of 1,2,3-trifluoropropane (**11**) generated by the *gauche g+* (~ 60°), the gauche *g-* (~ –60°) or the *anti* (~ 180°) orientations of the two consecutive F-C-C-F torsions. All the conformers remain within a narrow energy range of ~3 kcal/mol. In addition, some of the structures correspond to equally-stable conformational enantiomers (pair *g+/g+* and *g-/g-*, pair *g+/anti* and *anti/g-*, and pair *g-/anti* and *anti/g+*) and, accordingly, only the first conformer within each pair was considered for the IQA analysis. Since the relative energies for the **1-7** compounds are given as $\Delta E = E_{gauche} - E_{anti}$, the relative energies for CH_2F-CHF-CH_2F given in the text and in Figure 3 are similarly expressed as $\Delta E = E_{g+/g+} - E_i$ where *i* stands for any other conformer of **11**. Hence, a negative ΔE value means that conformer *i* is less stable than the *g+/g+* one.

Figure 3. Ball-and-stick representation of the different conformers obtained for 1,2,3-trifluoropropane (**11** in Scheme 1). F-C-C-F dihedral angles (º) and selected interatomic distances (Å) measured in the HF-D3/cc-pVTZ optimized structures (RI-MP2/cc-pVTZ in parentheses) are shown. Energy differences ($E_{g+/g+} - E_i$) in kcal/mol computed at the HF-D3/cc-pVTZ, RI-MP2/cc-pVTZ (in parentheses) and DLPNO-CCSD(T)/aug-cc-pVTZ [in brackets] levels of theory are also included.

g+/g+
ΔE= 0.00 (0.00) [0.00]

g+/g-
ΔE= -1.18 (-1.23) [-1.17]

g+/anti
ΔE= 0.17 (-0.14) [-0.18]

g-/g+
ΔE= -3.06 (-2.82) [-2.90]

g-/anti
ΔE= 0.74 (0.50) [0.39]

anti/anti
ΔE= -2.07 (-2.53) [-2.59]

Table 2 collects the IQF energy decomposition of the relative energies with respect to the reference *g+/g+* structure considering three molecular fragments (*i.e.*, P=CH$_2$F-, Q=-CHF-, and R=-CH$_2$F). In line with previous proposals, the parallel alignment of the C$_1$-F$_2$ and C$_8$-F$_9$ bonds in the less stable *g-/g+* and *anti/anti* conformers is associated to unfavorable electrostatic interactions between the corresponding CH$_2$F groups ($\Delta E_{\text{int},class}^{P \cdots R}$ of -2.4 and -2.1 kcal/mol, respectively), which are mainly ascribed to dipole-dipole repulsion ($\Delta E_{\text{int},class,dd}^{P \cdots R}$ of -2.0 and -2.1 kcal/mol for *g-/g+* and *anti/anti*). Hence, it seems reasonable to describe them as "1,3-dipole repulsions" in consonance with former suggestions.[9]

Table 2. IQF relative energy components (in kcal/mol) at the HF-D3/cc-pVTZ level for the energetically different conformers of 1,2,3-trifluoropropane (**11**). A three-fragment partitioning scheme (P=CH$_2$F, Q=CHF, and R=CH$_2$F) is assumed for the different structures. Energy differences are computed as $E_{g+/g+} - E_i$, so that a negative value means further stabilization of $g+/g+$.

	ΔE_{net}^P	ΔE_{net}^Q	ΔE_{net}^R	$\Delta E_{int,disp}$			$\Delta E_{int,xc}$			$\Delta E_{int,class}$			ΔE_{IQA}	$\Delta E_{HF\text{-}D3}$
				$P{\cdots}Q$	$P{\cdots}R$	$Q{\cdots}R$	$P{\cdots}Q$	$P{\cdots}R$	$Q{\cdots}R$	$P{\cdots}Q$	$P{\cdots}R$	$Q{\cdots}R$		
$\Delta E = E_{g+/g+} - E_{g+/g-}$	2.4	-1.9	0.6	-0.0	-0.1	0.0	0.6	-1.4	0.1	-0.3	-0.6	-0.9	-1.5	-1.2
$\Delta E = E_{g+/g+} - E_{g+/anti}$	0.7	-0.7	0.8	-0.0	-0.0	0.0	1.1	-0.2	-2.3	-0.4	-0.1	1.5	0.4	0.2
$\Delta E = E_{g+/g+} - E_{g-/g+}$	0.6	0.1	-1.4	0.0	-0.3	0.0	0.1	-0.7	-0.2	0.8	-2.4	0.2	-3.2	-3.1
$\Delta E = E_{g+/g+} - E_{g-/anti}$	0.4	1.3	-1.7	-0.0	0.0	0.0	0.5	1.0	-2.7	0.2	0.1	1.6	0.8	0.7
$\Delta E = E_{g+/g+} - E_{anti/anti}$	1.7	0.3	-0.5	-0.0	-0.3	0.0	-1.8	-1.1	-2.1	2.1	-2.1	1.6	-2.1	-2.1

The *gauche* effect is also expected to play a key role in determining the conformational landscape of 1,2,3-trifluoropropane. However, the missing *gauche* effects between vicinal fluorine atoms do not penalize the *anti/anti* structure as compared to the *g-/g+* one (*i.e.*, *anti/anti* is 1.0 kcal/mol more stable than *g-/g+* at HF-D3/cc-pVTZ). The lack of a net *gauche* effect in the *anti/anti* structure is revealed by IQF because the $\Delta E_{int,xc}$ terms between consecutive fragments favoring the *gauche* arrangement (-1.8 for $P{\cdots}Q$ and -2.1 kcal/mol for $Q{\cdots}R$) are nearly compensated by electrostatic interactions ($\Delta E_{int,class}$= 2.1 and 1.6 kcal/mol for $P{\cdots}Q$ and $Q{\cdots}R$) favoring the *anti* conformation. Other differences between the *g-/g+* and *anti/anti* structures arise in the intra-fragment net energies, that disfavor the *g-/g+* structure (ΔE_{net}^R =-1.4 kcal/mol) though they stabilize the *anti/anti* one (ΔE_{net}^P =1.7 kcal/mol).

The *g+/anti* and *g-/anti* conformers, with only one *gauche* arrangement, are nearly isoenergetic (*g+/anti*) or slightly more stable (*g-/anti*) than the reference *g+/g+* conformer presenting two *gauche* effects (see Figure 3). IQF confirms that the *gauche* effect at F$_6$-C$_5$-C$_8$-F$_9$ favors *g+/g+* over *g+/anti* and *g-/anti,* because the exchange-correlation $\Delta E_{int,xc}^{Q{\cdots}R}$ term (-2.3 and -2.7 kcal/mol for *g+/anti* and *g-/anti*, respectively*)* is greater in absolute value than the electrostatic $\Delta E_{int,class}^{Q{\cdots}R}$ term (1.5 kcal/mol for *g+/anti* and 1.6 kcal/mol for *g-/anti*). The same comparison involving the $\Delta E_{int,xc}^{P{\cdots}Q}$ and $\Delta E_{int,class}^{P{\cdots}Q}$ terms suggest that the *g+/anti* conformer may exhibit a reinforced gauche preference in the F$_2$-C$_1$-C$_5$-F$_6$ angle.

Inspection of the optimized geometries in Figure 3 suggests that C-H$\cdots$F contacts can contribute to the conformational energies. As expected, the formation/loss of the C-H$\cdots$F contacts can be traced back to modifications in either the deformation or the interaction IQA components involving the C-H$\cdots$F atoms (Table S4). The best fingerprint of the C-H$\cdots$F

contact is provided by the exchange-correlation $\Delta E^{AB}_{int,xc}$ energy between the F and H atoms because it scores among the largest $\Delta E^{AB}_{int,xc}$ terms and correlates well with the IQF exchange-correlation energy. For example, the reference *g+/g+* structure has an $H_4 \cdots F_9$ contact (2.57 Å) which is replaced by a similar $H_3 \cdots F_9$ interaction in the *g+/anti* conformer (2.53 Å), and this change is linked to significant interatomic $\Delta E^{AB}_{int,xc}$ contributions (-1.6 kcal/mol for $H_4 \cdots F_9$ and 1.9 kcal/mol for $H_3 \cdots F_9$ in Table S4). In the case of *g-/anti*, the $H_4 \cdots F_9$ interaction in *g+/g+* is preserved and one additional $F_2 \cdots H_{10}$ contact (2.49 Å) is formed that results in a favorable interatomic $F_2 \cdots H_{10}$ $\Delta E_{int,xc}$ contribution (2.3 kcal/mol in Table S4). Furthermore, the lack of 1,3 C-H$\cdots$F contacts in the *g+/g-* structure (*e.g.* $\Delta E_{int,xc}$ = -1.7 kcal/mol for $H_4 \cdots F_9$) can be invoked to explain its lower stability (1.2 kcal/mol with respect to *g+/g+)* in spite of maintaining two *gauche* effects. Hence, we conclude that the conformational properties of 1,2,3-trifluoropropane are more significantly influenced by through-space exchange-correlation interactions between fluorine and hydrogen atoms than the *gauche* effect between vicinal fluorine atoms, and that the IQA/IQF signature of these contacts is conveniently described in terms of the exchange-correlation interaction energies.

IQF analysis of fragments from an α,β-difluoro-γ-amino-acid

To help ascertain all the effects determining the conformational properties of the α,β-difluoro-γ-amino-acids **14a/14b** containing the -CHF-CHF- motif, we first examined compound **12** formally derived from **11** by replacing one fluorine atom by a polar amide group (see Scheme 1). Either a *gauche* or an *anti* orientation in the adjacent C-F bonds and a *cis* or a *trans* arrangement for the vicinal C-F and C=O bonds can appear in **12** (see Figure 4). Only five conformers were located on the HF and MP2 potential energy surfaces (*g-/cis* turned out to be unstable). Their relative energies given in Figure 4 are expressed as $\Delta E = E_{g+/trans} - E_i$ where *i* stands for any other conformer of **12**.

The positioning of the –(C=O)NHCH$_3$ group in **12** results in a strong conformational selection in favor of the *g+/trans* or *g-/trans* conformers, which is unequivocally interpreted by the three-fragment (*P*=CH$_2$F, *Q*=CHF, and *R*=CONHCH$_3$) IQF partitioning. As already observed in **10**, the *cis* alignment in the adjacent C_5-F_6 and C_8=O_9 bonds in **12** is clearly destabilized by the classical electrostatic interaction between fragments *Q* and *R*. The

corresponding $\Delta E_{\text{int,class}}^{Q\cdots R}$ values are -7.5 and -8.4 for the *g+/cis* and *anti/cis* conformers, the exchange-correlation $\Delta E_{\text{int,xc}}^{Q\cdots R}$ being also unfavorable (see Table 3). Some differences appear in the $P\cdots Q$ and $P\cdots R$ interaction terms that contribute to the relative stability of the *g+/cis* and *anti/cis* conformers. Thus, the lack of *gauche* effect between vicinal C-F bonds makes *anti/cis* less stable than *g+/trans* (*e.g.*, $\Delta E_{\text{int,xc}}^{P\cdots Q} + \Delta E_{\text{int,class}}^{P\cdots Q}$ =-2.8 + 1.5= -1.3 kcal/mol). On the other hand, the terminal $P\cdots R$ interaction through a $F_2\cdots H_{11}$-N_{10} contact favors *anti/cis* ($\Delta E_{\text{int,xc}}^{P\cdots R}$=3.0 kcal/mol and $\Delta E_{\text{int,class}}^{P\cdots R}$=3.4 kcal/mol) over *g+/cis* ($\Delta E_{\text{int,xc}}^{P\cdots R}$=0.4 kcal/mol and $\Delta E_{\text{int,class}}^{P\cdots R}$=-2.0 kcal/mol). With respect to the electrostatic terms, the partial alignment of the C_1-F_2 and amide dipole moments contributes to further destabilize *g+/cis* (the $P\cdots Q$ dipole-dipole interaction amounts to -1.7 kcal/mol).

Figure 4. Ball-and-stick representation of the five conformers optimized for 2,3-difluoro-*N*-methylpropanamide (**12** in Scheme 1). F-C-C-F and F-C-C-C=O dihedral angles (º) and selected interatomic distances (Å) measured in the HF-D3/cc-pVTZ optimized structures (RI-MP2/cc-pVTZ in parentheses) are included. Energy differences ($E_{g+/trans} - E_i$) in kcal/mol computed at the HF-D3/cc-pVTZ, RI-MP2/cc-pVTZ (in parentheses) and DLPNO-CCSD(T)/aug-cc-pVTZ [in brackets] levels of theory are also included.

g+/trans ΔE= 0.00 (0.00) [0.00]   **g-/trans** ΔE= -0.25 (-0.18) [-0.26]   **anti/trans** ΔE= -4.18 (-4.04) [-3.95]

g+/cis ΔE= -8.05 (-7.61) [-7.51]   **anti/cis** ΔE= -5.52 (-5.34) [-5.18]

The magnitude of the relative energy of the *anti/trans* conformer of **12** (4.2 kcal/mol) as compared to the *g+/trans* structure is difficult to explain only in terms of the small *gauche* effect estimated as $\Delta E_{int,xc}^{P\cdots Q} + \Delta E_{int,class}^{P\cdots Q}$ =-3.4 + 2.9= -0.5 kcal/mol. In contrast, the terminal $P\cdots R$ interactions, $\Delta E_{int,xc}^{P\cdots R}$ =-1.6 kcal/mol and $\Delta E_{int,class}^{P\cdots R}$ =-2.6 kcal/mol, make a more significant contribution to the destabilization of *anti/trans*. These terms can be associated with the loss of the $H_3\cdots O_9$ contact ($\Delta E_{int,xc}^{H_3\cdots O_9}$ =-2.1 kcal/mol in Table S5) when comparing *g+/trans* with *anti/trans*, while the electrostatic contribution can be connected to the partial alignment of the P and R dipole moments in the *anti/trans* structure (the $P\cdots R$ dipole-dipole interaction amounts to -2.6 kcal/mol). Thus, we see again that either 1,3 dipole-dipole interactions or O/F⋯H contacts can be more determining than the *gauche* effect between adjacent C-F groups.

Table 3. IQF energy components at the HF-D3/cc-pVTZ level for the energy difference (kcal/mol) among the five conformers optimized for 2,3-difluoro-*N*-methylpropanamide (**12**). A three-fragment partitioning scheme (P=CH$_2$F-, Q=-CHF-, and R=-CONHCH$_3$) is assumed for the different conformers. Energy differences are computed as $E_{g+/trans} - E_i$, so that a negative value means further stabilization of *g+/trans*.

	ΔE_{net}^{P}	ΔE_{net}^{Q}	ΔE_{net}^{R}	$\Delta E_{int,disp}$			$\Delta E_{int,xc}$			$\Delta E_{int,class}$			ΔE_{IQA}	ΔE_{HF-D3}
				$P\cdots Q$	$P\cdots R$	$Q\cdots R$	$P\cdots Q$	$P\cdots R$	$Q\cdots R$	$P\cdots Q$	$P\cdots R$	$Q\cdots R$		
$\Delta E = E_{g+/trans} - E_{g-/trans}$	-0.8	-1.7	0.6	0.0,	-0.1,	0.0	-0.1,	-0.4,	1.3	0.0,	0.4,	-0.0	-0.7	-0.2
$\Delta E = E_{g+/trans} - E_{anti/trans}$	0.1	-1.7	0.7	-0.0,	-0.4,	0.0	-3.4,	-1.6,	1.7	2.9,	-2.6,	-0.1	-4.3	-4.2
$\Delta E = E_{g+/trans} - E_{g+/cis}$	1.1	1.7	2.0	-0.0,	0.3,	-0.4	-0.5,	0.4,	-4.8	0.4,	-2.0,	-7.5	-9.3	-8.0
$\Delta E = E_{g+/trans} - E_{anti/cis}$	0.3	0.3	0.1	0.0,	0.6,	-0.4	-2.8,	3.0,	-3.9	1.5,	3.4,	-8.4	-6.3	-5.5

In contrast with the case of compound **12**, the positioning of the bulky isoindole-1,3-dione group –(C=O)NHCH$_3$ group in **13** has a minor conformational influence. For this reason, its analysis is reported in the Supplementary Material (Figure S1 and Tables S6-S7).

*Conformational analysis and QM calculations on the **14a** and **14b** dipeptides*

The QM and IQA calculations on the model compounds **1-13** characterize several conformational effects (*gauche/anti, cis/trans,* through space F⋯H, dispersion attractions, etc.) than can act simultaneously in the **14a/14b** dipeptides. To better assess these and other effects, we investigated first whether or not additional conformations to those observed in the **14a/14b** crystal structures could be accessible. Thus, we performed an automated conformational search followed by HF-D3/cc-pVTZ geometry optimizations of the resulting

conformers in the gas-phase and in the solvent continuum (see Tables S8-S9 and Figures S2-S3).

Most remarkably, inspection of the optimized geometries and relative energies of the **14a** and **14b** conformers reveals that the X-ray conformations (labelled as **14a-conf1** and **14b-conf1**) are indeed among the most stable ones in the gas-phase and in the chloroform solution. In addition, we found that the structures presenting the expected F_{23}-C_{22}-C_{19}-F_{20} and F_{20}-C_{19}-C_{16}-N_{13} *gauche* orientation and the *trans* F_{23}-C_{22}-C_{25}=O_{26} arrangement (see Figure 5 for atom numbering) are, in general, energetically favored as expected by common assumptions. There are, however, low energy conformers, especially for **14a**, that do not present the expected *gauche* orientation around the fluorine atoms (see for instance **14a-conf4** and **14a-conf5**). Moreover, it turns out that the conformer **14a-conf6** is not drastically penalized in the gas-phase despite presenting a *cis* F_{23}-C_{22}-C_{25}=O_{26} alignment and an almost *anti* orientation for the F_{23}-C_{22}-C_{19}-F_{20} and F_{20}-C_{19}-C_{16}-N_{13} bonds.

The results of our conformational search can be addressed with NMR experimental data. Thus, the NMR spectra of **14a** and **14b** have been recorded at 300 K in deuterated chloroform solution and their coupling constants determined by simulation/iteration sequences.[14] We also estimated $^3J_{HF}$ coupling constants around the FC_{22}-$C_{19}F$ bond using a Karplus-type relation[51] for the five most stable conformers of **14a** and **14b**, and the corresponding values were Boltzmann-averaged at 300 K according to the HF-D3/cc-pVTZ relative energies in chloroform (Table S10). For **14a**, the favorable comparison between the computed and experimental values validates the results of our conformational analysis (the computational averages for $^3J_{FH}$ ($F_{23}H_{21}$) and $^3J_{HF}$ ($H_{24}F_{20}$) are 27.4 and 28.2 *Hz* compared with the experimental ones of 27.0 and 28.9 *Hz*). It is interesting to note that some conformational variability of **14a** in chloroform solution can be expected because the ΔE difference between the two most stable conformers is not large (1.0 kcal/mol). For **14b**, the agreement between the estimated coupling constants and the experimental ones is only moderate (the calculated averages for $^3J_{FH}$ and $^3J_{HF}$ are 26.1 and 13.0 *Hz* while the experimental values are 23.0 and 21.4 *Hz*). However, the computed $^3J_{FH}$ and $^3J_{HF}$ values for **14b-conf1** (30.8 and 8.1) and **14b-conf2** (6.6 and 31.7) would approach to the experimentally-derived ones (23.0 and 21.4) upon averaging, provided that these two conformers become nearly isoenergetic. Although the calculated ΔE value between **14b-conf1** and **14b-conf2** is already small (0.7 kcal/mol), it is likely that method/basis-set

improvements in the QM level of theory and/or a better description of thermal and solvation effects would be required to increase the agreement with experimental data.

*IQF assessment of the conformational effects acting upon **14a***

Our QM calculations suggest that intramolecular factors largely determine the conformational preferences of **14a/14b** as their low-energy conformers in the gas-phase are quite close to their crystallographic structures. Moreover, the intrinsic stability of the two diastereomers is similar and we expect that the same local effects influence their conformational energies. Taking also into account the large computational cost of the IQA calculations on these systems, we focused on the IQA analysis of the relative stability of selected **14a** conformers. Thus, we performed IQA calculations on **14a-conf1** and **14a-conf2**, which are two different *gauche* forms (*g+* and *g-*, respectively) that interconvert into each other through a ~120º rotation about the $F_{23}C_{22}–C_{19}F_{20}$ bond. We also selected conformer **14a-conf5**, which shows an *anti* conformation at $F_{23}–C_{22}–C_{19}–F_{20}$, and conformer **14a-conf6**, which is a helical-type compact structure presenting all *anti* ($F_{23}-C_{22}-C_{19}-F_{20}$ and $F_{20}-C_{19}-C_{16}-N_{13}$) and *cis* ($F_{23}-C_{22}-C_{25}=O_{26}$) arrangements (see Figure 6). Table 5 summarizes the IQF decomposition of the HF-D3/cc-pVTZ relative energies involving a four-fragment $O\text{-}P\text{-}Q\text{-}R$ partitioning in which fragments P and Q correspond to the central $C_{22}HF$ and $C_{19}HF$ units, respectively, fragment O comprises the Ace-CH(Ph)-NHCO– residue and fragment R contains the isoindole-1,3-dione moiety. The relative energies are now expressed as $\Delta E = E_{14a\text{-}conf1} − E_{14a\text{-}confi}$ where i=2, 5, or 6.

Figure 5. Ball-and-stick representation of selected conformers optimized for **14a** at the HF-D3/cc-pVTZ level of theory. F-C-C-F, F-C-C-N, and F-C-C-C=O dihedral angles (°) and selected interatomic distances (Å) measured in the HF-D3/cc-pVTZ gas phase optimized structures are included. Energy differences ($E_{14a\text{-conf1}} - E_{14a\text{-confi}}$) in kcal/mol computed at the HF-D3/cc-pVTZ level of theory in the gas-phase and in chloroform (in Italics) are also included.

14a-conf1 ΔE= 0.00 *0.00*   **14a-conf2** ΔE= 0.74 *-1.05*

14a-conf5 ΔE= -1.97 *-2.14*   **14a-conf6** ΔE= -2.64 *-4.13*

We first analyze the variation of the F_{23}-C_{22}-C_{19}-F_{20} dihedral from 67.5° in conformer **14a-conf1** to -58.4° in **14a-conf2**, affecting the relative positioning of the O and R fragments (see Figure 5). As the two conformers are presumably stabilized by a similar *gauche* effect and the placement of the terminal isoindole-1,3-dione group in R with reference to the central P-Q fragments has little influence, their energy difference in the gas-phase is quite small, 0.7 kcal/mol at the HF-D3/cc-pVTZ level favoring **14a-conf2**. Nonetheless, examination of the IQF terms collected in Table 4 reveals some fine details concerning this energy difference. On one hand, there are some indications about a more stabilizing *gauche* effect in **14a-conf2** given that $\Delta E_{\text{int,xc}}^{P\cdots Q} + \Delta E_{\text{int,class}}^{P\cdots Q}$ =1.5 - 0.9= 0.6 kcal/mol. On the other one, IQF reveals substantial energy compensation occurring upon the formation of new $O\cdots R$ contacts with simultaneous

loss of $P{\cdot}{\cdot}R$ and $Q{\cdot}{\cdot}{\cdot}R$ ones. Thus, the exchange-correlation interaction between fragments O and R largely stabilizes **14a-conf2** (17.6 kcal/mol, comprising specific $H_{17}{\cdot}{\cdot}{\cdot}O_{26}$=5.0 kcal/mol, $C_{16}{\cdot}{\cdot}{\cdot}O_{26}$=3.1, $O_{12}{\cdot}{\cdot}{\cdot}H_{42}$=3.0 and $O_{12}{\cdot}{\cdot}{\cdot}H_{44}$=2.3 pair interactions; see Figure 5 and Table S11). This attractive component is partly neutralized by the equivalent terms accounting for the $O{\cdot}{\cdot}{\cdot}Q$ and $P{\cdot}{\cdot}{\cdot}R$ fragment interactions, which are -7.6 and -4.4 kcal/mol, respectively, reflecting the loss of the $F_{20}{\cdot}{\cdot}{\cdot}H_{44}$ and $H_{21}{\cdot}{\cdot}{\cdot}O_{26}$ contacts (-3.2 and -2.2 kcal/mol) and the $F_{23}{\cdot}{\cdot}{\cdot}H_{18}$ and $F_{23}{\cdot}{\cdot}{\cdot}C_{16}$ ones (-2.0 and -1.8 kcal/mol). In addition, the shortening of the $O{\cdot}{\cdot}{\cdot}R$ distance in **14a-conf2** implies not only stabilizing inter-fragment energy contributions, but also a large intra-fragment distortion as in the case of intermolecular complexes. For example, the ΔE_{net}^{R} term destabilizes **14a-conf2** by 9.7 kcal/mol. Altogether, these IQA components allow us to energetically weigh the formation/loss of intramolecular contacts upon the **14a-conf1→14a-conf2** transition, which nearly compensate each other.

Table 4. IQF energy components at the HF-D3/cc-pVTZ level for the energy difference (kcal/mol) among selected conformers optimized for compound **14a**. A four-fragment partitioning scheme (O = $CH_3OCOCH(CH_2Ph)NHCO$-, P = -CHF-, Q = -CHF-, and R = -CH_2-isoindol-1,3-dione) is assumed for the different conformers. Relative energies are given as $E_{14a\text{-}conf1} - E_{14a\text{-}confi}$ so that a negative value means further stabilization of *14a-conf1*.

	ΔE_{net}^{O}	ΔE_{net}^{P}	ΔE_{net}^{Q}	ΔE_{net}^{R}	$\Delta E_{int,disp}$			$\Delta E_{int,xc}$			$\Delta E_{int,class}$			ΔE_{IQA}	$\Delta E_{HF\text{-}D3}$
					$P{\cdot}{\cdot}Q$	$P{\cdot}{\cdot}R$	$O{\cdot}{\cdot}P$	$P{\cdot}{\cdot}Q$	$P{\cdot}{\cdot}R$	$O{\cdot}{\cdot}P$	$P{\cdot}{\cdot}Q$	$P{\cdot}{\cdot}R$	$O{\cdot}{\cdot}P$		
					$Q{\cdot}{\cdot}R$	$O{\cdot}{\cdot}Q$	$O{\cdot}{\cdot}R$	$Q{\cdot}{\cdot}R$	$O{\cdot}{\cdot}Q$	$O{\cdot}{\cdot}R$	$Q{\cdot}{\cdot}R$	$O{\cdot}{\cdot}Q$	$O{\cdot}{\cdot}R$		
$\Delta E = E_{14a\text{-}conf1} - E_{14a\text{-}conf2}$	-5.5	-1.2	2.8	-9.7	0.3, -0.8, 0.1			1.5, -4.4, 1.6			-0.9, -1.1, -0.8			0.3	0.7
					0.2, -0.9, 4.5			0.2, -7.6, 17.6			0.8, -1.0, 4.7				
$\Delta E = E_{14a\text{-}conf1} - E_{14a\text{-}conf5}$	-17.5	-1.0	4.5	-19.8	0.3, -0.9, 0.1			-2.5, -4.5, 2.2			2.8, -1.2, 0.5			-2.2	-2.0
					-0.4, -1.8, 12.5			-0.5, -9.6, 35.2			-0.2, -3.2, 2.8				
$\Delta E = E_{14a\text{-}conf1} - E_{14a\text{-}conf6}$	-16.9	-3.4	3.2	-21.7	0.3, 0.7, -0.4			-1.5, 1.1, -2.4			2.5, -0.1, -6.7			-2.1	-2.6
					-0.7, -0.8, 10.8			-4.6, -4.9, 33.7			2.0, 1.1, 6.5				

More interesting conformational effects act upon **14a-conf5**, whose overall shape differs significantly with respect to those of **14a-conf1/14a-conf2**. There is an *anti* F_{23}-C_{22}-C_{19}-F_{20} arrangement in **14a-conf5,** which is 2.0 kcal/mol less stable than **14a-conf1** at HF-D3/cc-pVTZ. However, this energy difference cannot be assigned to the loss of the *gauche* F_{23}-C_{22}-C_{19}-F_{20} effect, because the IQF exchange-correlation term favoring the *gauche* orientation ($\Delta E_{int,xc}^{P{\cdot}{\cdot}{\cdot}Q}$=-2.5 kcal/mol) is completely canceled out by the electrostatic term ($\Delta E_{int,class}^{P{\cdot}{\cdot}{\cdot}Q}$=2.7 kcal/mol) favoring the *anti* one. Likewise the *g+/g+* and *anti/anti* pair in **11**, the exchange-correlation stabilization of the gauche F-C-C-F arrangement in **14a-conf1** is reversed by the electrostatic term favoring the *anti* orientation in **14a-conf5**, what is in contrast with the results obtained for the small models **1-5**. Hence, the destabilization of **14a-**

conf5 with reference to **14a-conf1** is better rationalized in terms of the forming/breaking of intramolecular contacts. Thus, the intermediate distance (5.1 Å) between the center of mass of the aromatic rings in fragments O and R with an almost parallel arrangement of the ring planes (12.1º) may allow some π–π favorable interaction in **14a-conf5**, whereas the loss of the CH$\cdots$F contacts characteristic of **14a-conf1** would disfavor it. The energetic impact of these structural changes can be assessed through the IQF components. One the one hand, the approaching of the terminal $O\cdots R$ groups gives large and stabilizing values for the $\Delta E_{\text{int,disp}}^{O\cdots R}$ (12.5 kcal/mol) and $\Delta E_{\text{int,xc}}^{O\cdots R}$ (35.2 kcal/mol) terms. The $\Delta E_{\text{int,xc}}^{O\cdots R}$ value stems from many inter-atomic contributions involving the –CH$_2$-N moiety in fragment R and the amide and phenyl groups in fragment O (*e.g.*, H$_{18}\cdots$O$_{26}$ 3.6 kcal/mol, N$_{13}\cdots$C$_{39}$ 2.6 kcal/mol, C$_{16}\cdots$O$_{26}$ 2.2 kcal/mol, H$_{17}\cdots$C$_{35}$ 2.1 kcal/mol, etc.). The closer $O\cdots R$ contacts are accompanied by opposite intra-fragment distortion effects for the O and R moieties (-17.5 and -19.8 kcal/mol) so that the sum $\Delta E_{net}^{O} + \Delta E_{net}^{R} + \Delta E_{\text{int,disp}}^{O\cdots R} + \Delta E_{\text{int},xc}^{O\cdots R}$ amounts to 10.4 kcal/mol favoring **14a-conf5**. On the other hand, this contribution is overcompensated by the penalty associated with the loss of the contacts exhibited by **14a-conf1** (C$_{16}$-H$_{18}\cdots$F$_{23}$, F$_{20}\cdots$H$_{44}$, and H$_{21}\cdots$O$_{26}$, see Figure 6) that is mainly accounted for by $\Delta E_{\text{int,xc}}^{P\cdots R}$=-4.5 and $\Delta E_{\text{int,xc}}^{O\cdots Q}$=-9.6 kcal/mol, determining thus the lower stability of **14a-conf5**.

As previously noticed, the *cis* F-C-C=O arrangement in **10** or **12** implies a large destabilization of more than 5 kcal/mol with respect to the *trans* orientation, basically due to the dipole-dipole interaction between the F-C and C=O groups. We see in Figure 6 that **14a-conf6** has a *cis* F$_{23}$-C$_{22}$-C$_{25}$=O$_{26}$ orientation and two *anti* F$_{23}$-C$_{22}$-C$_{19}$-F$_{20}$ and F$_{20}$-C$_{19}$-C$_{16}$-N$_{13}$ groups, but it is only 2.6 kcal/mol less stable than **14a-conf1**. Nevertheless, the impact of the *cis* F$_{23}$-C$_{22}$-C$_{25}$=O$_{26}$ dihedral in the electrostatic $\Delta E_{\text{int,class}}^{O\cdots P}$ value is -6.7 kcal/mol, which is similar to those observed in **10** or **12**. The *gauche* effect is again reversed in the **14a-conf1**/**14a-conf6** pair as the sum $\Delta E_{\text{int,xc}}^{P\cdots Q} + \Delta E_{\text{int,class}}^{P\cdots Q}$ equals to 1.0 kcal/mol. Further stabilization of **14a-conf6** comes from the various $O\cdots R$ interactions between the bulky terminal fragments, partially compensating the unfavorable *cis* F-C-C=O orientation. These interactions can be measured in terms of the sum $\Delta E_{net}^{O} + \Delta E_{net}^{R} + \Delta E_{\text{int,disp}}^{O\cdots R} + \Delta E_{\text{int,xc}}^{O\cdots R}$ = 5.9 kcal/mol. In addition, only one of the two CH$\cdots$F contacts is lost upon the **14a-conf1**→**14a-conf6** transition, determining an energy change $\Delta E_{\text{int,xc}}^{P\cdots R} + \Delta E_{\text{int,xc}}^{O\cdots Q}$ = -3.8 kcal/mol, which does not neutralize the global effect of the $O\cdots R$ contacts. Therefore, IQF shows how the *a priori* strong preference for the *trans*

F-C-C=O conformation in the **14a-conf1/14a-conf6** pair is significantly reduced by the unexpected reversal of the *gauche* effect and the corresponding balance of interactions between the terminal groups.

Discussion and Conclusions

Among the major conformational effects associated with C-F bonds, the *gauche* preference in F-C-C-X moieties (X=F, O, N, or C), the repulsion between C-F bonds aligned parallel in 1,3-positions, and the favored *trans*-planar arrangement in F-C-C=O moieties, are usually invoked to rationalize or foresee conformations in fluorine containing systems. However, either X-ray structures or NMR measurements have revealed molecular conformations that differ from those expected according to the usual fluorine effects.[15] Moreover, two possible *gauche* orientations (+60°/-60°) are accessible to F-C-C-X moieties, which in most cases result in different molecular conformations. Hence, additional intramolecular interactions and environmental effects may play a significant role in order to explain the conformational preferences of fluorinated molecules. To gain further understanding of such effects, IQA, as a reference-free energy decomposition method, can be useful to express the conformational energies predicted by QM calculations into unambiguously contributions, which include electrostatic and exchange-correlation interatomic interactions.

Concerning the prototypical *gauche* effect in 1,2-difluoroethane, the IQA method has been formerly employed[24] to highlight specifically the *gauche* stabilization due to the 1,3 Coulombic attraction between C and F atoms. However, we note that there are strong F···F and C···C repulsions as characterized by IQA that can be seen to compensate the C···F attractive energies. Moreover, the larger C-C-F angles and C···F distances obtained in the *gauche* form as compared to the *anti* one (110.3/108.1° and 2.34/2.32 Å) seem not compatible with explaining the *gauche* effect as the consequence of the 1,3 electrostatic attraction between C and F atoms. In addition, we also consider that other terms like the C···C and C···F exchange-correlation interactions contribute to the *gauche* stability. Thus, when the IQA atomic terms are grouped by defining two interacting CH_2F fragments separated by the rotatable bond, it emerges that the *gauche* structure is stabilized by the exchange-correlation interaction and destabilized by the electrostatic $CH_2F···CH_2F$ tem, involving only a minor distortion at each fragment. In this fragment-based IQF analysis, the electrostatic interaction can be further decomposed to show how the *gauche* destabilization is partially due to dipole-dipole repulsion, the dipoles being mainly associated to the C-F

bonds. We believe that the IQF interpretation of the *gauche* effect in 1,2-difluoroethane is more chemically appealing and, accordingly, we apply it to the rest of molecules considered in this work. We also note that, regardless of atomic contributions being grouped or not, IQA clearly shows that both electrostatic and exchange-correlation interactions should be considered to explain the *gauche* effect in 1,2-difluorethane.

Examination of the 1,2-difluoroethane related systems **2-7** bearing different polar/charged substituents points out that the quantum exchange-correlation inter-fragment interaction systematically stabilizes the *gauche* conformation. In contrast, the electrostatic interaction term is system-dependent because the sign and magnitude of $\Delta E_{\text{int,class}}^{P \cdots Q}$ is mainly determined by the particular interaction(s) between the fluorine atom in fragment P and the closest atoms in fragment Q. For the positively charged systems, the exchange-correlation and the classical electrostatic inter-fragment interactions are large and comparable, which contrasts with previous assumptions explaining their *gauche* preference only in terms of electrostatic effects. IQF also emphasizes that the magnitude and nature of the electrostatic interactions depends on the particular characteristics of the charged moiety.

As previously proposed,[9] dipole-dipole interaction arises as the main contribution to the stability of the *trans*-planar F-C-C=O arrangement in the CH_2F-COX molecules (**8-10**). However, the exchange-correlation term is also relevant for the ketone (**8**) and the amide (**10**) derivatives. More particularly, the interatomic F$\cdots$HN interaction in **10** makes a large contribution to the $\Delta E_{\text{int,xc}}^{P \cdots Q}$ term. This relatively large exchange-correlation interaction between fluorine and nearby hydrogen atoms, also observed in 3-fluoropropanal (**3**) and 2-fluoroethan-1-aminium (**6**), can be considered as the signature for a (weak) hydrogen bond. Fluorine is considered a poor hydrogen bonding acceptor although there are examples of crystal structures showing short intramolecular contacts between organic fluorine and HO-/HN-moieties[9, 57] that have been assumed to result almost exclusively from dipole-dipole electrostatic interactions, excepting for F$\cdots$HC contacts where it is thought that dispersion also plays a role. Nonetheless, our calculations help clarify the nature and impact of these F$\cdots$HN and F$\cdots$HC contacts that particularly affect the quantum mechanical interaction between the H-bonded groups, in line with recent $^4J_{HF}$ measurements and NBO calculations performed for α-fluoro amides.[30] Thus, we conclude that the largest exchange-correlation IQA energies help identify the relevant F$\cdots$HC/HN interactions.

To analyze the various fluorine effects in more complex settings, we examined all the possible conformations in 1,2,3-trifluoropropane (**11**) and two other compounds (**12** and **13**) related to **14a/14b**. The two less stable conformers obtained for 1,2,3-trifluoropropane present the unfavorable parallel alignment of 1,3 C-F bonds previously described in polyfluorinated alkanes.[9] IQF confirms the appearance of an unfavorable electrostatic interaction between the 1,3 CH_2F groups and ascribes it to dipole-dipole repulsion. But unexpectedly, the most stable conformer obtained for 1,2,3-trifluoropropane does not result from maximizing the number of *gauche* effects and minimizing the 1,3 dipole-dipole repulsions. According to our analyses, the presence of 1,3 F···H-C interactions also contributes to explain the relative stability of the conformers. These F···H-C contacts are among the largest exchange-correlation interatomic interactions in 1,2,3-trifluoropropane and their stabilizing effect is larger than the *gauche* effect. The partial alignment of the amide dipole with a C-F bond and the presence of different F···H contacts also explain the conformational landscape obtained for 2,3-difluoro-*N*-methylpropanamide (**12**).

The various analyses carried out on the model systems may help us to better ascertain the various effects determining the conformational properties of the difluorinated dipeptide **14a** and **14b** diastereomers. According to X-ray crystallography, the (*R,R*) or (*R,S*) stereochemistry for the fluorination at the central C_{22} and C_{19} atoms leads to a different backbone conformation for the whole molecule.[14] In the two crystal structures, the vicinal C_{22}-F_{23}/C_{19}-F_{20} and C_{19}-F_{20}/C_{16}-N_{13} bonds are in *gauche* while the C_{22}-F_{23} bond aligns antiparallel to the adjacent amide carbonyl, which seems in consonance with expectations. The QM-refined conformational search performed for **14a/14b** predicts that the lowest energy conformer either in the gas-phase or in the solvent-continuum is structurally close to the crystallographic structure. This seems to indicate that crystal packing and solvent effects would play only a minor role in the conformational preferences of **14a/14b**, the intramolecular factors being dominant. However, the conformational search illustrates that the observed crystal structures are not the only conformers compatible with the effects usually assigned to fluorine atoms. For instance, two alternative *gauche* forms (*g+* or *g-*) could be accessible for the vicinal C_{22}-F_{23}/C_{19}-F_{20} and C_{19}-F_{20}/C_{16}-N_{13} bonds in the gas-phase or in solution. This seems confirmed by our estimations of the $^3J_{HF}$ values in chloroform obtained for the vicinal fluorine and hydrogen atoms bound to C_{22}/C_{19} in **14a/14b**, which are in reasonable agreement with experimental data. Moreover, the energetic penalty associated to the presence of unfavorable *anti* or *cis* arrangements around the fluorine atoms is not dramatic (*e.g.*, 2.5

kcal/mol), pointing thus towards the compensating roles of other stabilizing intra-molecular interactions.

The IQA energy decomposition can treat relatively large molecules like the selected conformers of **14a**. Three of them differ in the *g+*, *g-*, or *anti* arrangement of the F_{23}-C_{22}-C_{19}-F_{20} moiety, whereas the fourth one presents the less favorable F_{23}-C_{22}-C_{19}-F_{20} and F_{20}-C_{19}-C_{16}-N_{13} *anti* and F_{23}-C_{22}-C_{25}=O_{26} *cis* orientations. In all the cases, the careful examination of the IQF descriptors allows us to assess the energetic impact of the *gauche/anti* and *cis/trans* effects. In comparison with the smaller model systems **8-10** and **12**, IQF indicates that the important electrostatic F-C-C=O *trans* preference (~6-8 kcal/mol) is appreciably transferable. Interestingly, the exchange-correlation and electrostatic balance favoring the *gauche* F-C-C-F orientation can be altered in some of the **14a** conformers (also in **11** conformers) resulting in a small inverted *gauche* effect (<1.0 kcal/mol) that benefits the *anti* F-C-C-F arrangement. Furthermore, our four-fragment IQA partitioning points out that the formation/rupture of other intramolecular contacts (*e.g.*, $\pi\cdots\pi$, F$\cdots$H-C, etc.) can modulate and/or attenuate the F-C-C=O *trans* and the F-C-C-F *gauche* effects. Therefore, our results stress that the *gauche* effect can be both system and conformation dependent, what is in consonance with previous studies[19, 26-28] showing that environmental (solvent) effects can modulate or alter the *gauche* conformational preference.

In summary, our QM calculations complemented with the HF-D3 IQF energy decompositions are useful to analyze in a systematic and consistent manner the energetic preferences of small fluorinated compounds having either *gauche/anti* or *cis/trans* conformations. Following the IQF approach, we find a clear correspondence between specific exchange-correlation and/or electrostatic fragment-interaction energies with the appearance of the *gauche/anti* or *cis/trans* effects, providing also insight into their magnitude and nature. The same IQF approach can be extended to assess those *gauche/anti* or *cis/trans* effects in molecules with two or more rotatable bonds as well as to study the roles played by other concomitant effects (*e.g.*, specific CH/OH/NH$\cdots$F contacts, 1-3 electrostatic interactions, etc.). For the relatively large α,β-difluoro-γ-amino acid derivatives, our conformational search followed by QM and selected IQF calculations complement well their crystallographic and NMR characterization. The conformational preferences of these compounds as detailed by the theoretical analysis point out that the *gauche/anti* and *cis/trans* effects associated to fluorine bonds may be attenuated in large molecules, where the most preferred conformations may be dictated by other non-fluorine specific intra-molecular interactions.

Finally, we note that similar computational protocols including solvent effects could help in the rational design of fluorinated molecules having a nearly frozen conformation tailored for a particular application. This is still a challenging task as most of the fluorinated compounds have emerged from broad chemical screening programs and the actual influence of fluorine is considered retrospectively.[9] However, the QM and IQF assessments of the conformational effects associated to the presence of fluorine atoms (*gauche* effect, the 1,3 C-F repulsion and other electrostatic interactions, the hydrogen bond acceptor capability of organic fluorine, etc.) could result in new guidelines to predict the conformation of structurally-complex fluorinated molecules.

Acknowledgments

Electronic Supplementary Information

Table S1 with the sum of the different IQA atomic contribution for the small (**1-10**) models. Tables S2-S5 and S11 with the largest changes in the IQA atomic contributions for the different systems. Figure S1 with a representation of the different conformers obtained for **13** and their relative energies. Table S6 and S7 with IQF and the largest changes in the IQA atomic contributions and results obtained for **13**. Tables S8 and S9 with energies and geometrical parameters obtained for the different conformers optimized for **14a** and **14b**. Figures S2 and S3 with a ball-and-stick representation of the different conformers optimized for **14a** and **14b**. Table S10 with the $^3J_{H,F}$ coupling constants estimated for some of the **14a** and **14b** conformers. Table S12 with the equivalence between the filenames with the Cartesian coordinates (COORD.zip) and the HF/MP2 optimized compounds. Table S13 comparing the HF-D3 IQF and correlated IQF results for 1,2-difluoroethane.

References

1. Y. Zhou, J. Wang, Z. Gu, S. Wang, W. Zhu, J. L. Aceña, V. A. Soloshonok, K. Izawa and H. Liu, *Chem. Rev.*, 2016, 116, 422-518.
2. P. Jeschke, *ChemBioChem*, 2004, 5, 570-589.
3. T. Fujiwara and D. O'Hagan, *J. Fluor. Chem.*, 2014, 167, 16-29.
4. P. Kirsch, *J. Fluor. Chem.*, 2015, 177, 29-36.
5. J. H. Yun, S. Park, J. H. Heo, H.-S. Lee, S. Yoon, J. Kang, S. H. Im, H. Kim, W. Lee, B. Kim, M. J. Ko, D. S. Chung and H. J. Son, *Chem. Sci.*, 2016, 7, 6649-6661.
6. L. E. Zimmer, C. Sparr and R. Gilmour, *Angew. Chem. Int. Ed.*, 2011, 50, 11860-11871.
7. D. Cahard and V. Bizet, *Chem. Soc. Rev.*, 2014, 43, 135-147.
8. A. A. Berger, J.-S. Völler, N. Budisa and B. Koksch, *Acc. Chem. Res.*, 2017, 50, 2093-2103.
9. D. O'Hagan, *Chem. Soc. Rev.*, 2008, 37, 308-319.
10. H.-J. Böhm, D. Banner, S. Bendels, M. Kansy, B. Kuhn, K. Müller, U. Obst-Sander and M. Stahl, *ChemBioChem*, 2004, 5, 637-643.
11. J. W. Banks, A. S. Batsanov, J. A. K. Howard, D. O'Hagan, H. S. Rzepa and S. Martin-Santamaria, *J. Chem. Soc., Perkin Trans. 2*, 1999, 2409-2411.
12. M. Schüler, D. O'Hagan and A. M. Z. Slawin, *Chem. Commun.*, 2005, 4324-4326.
13. L. Hunter, P. Kirsch, A. M. Z. Slawin and D. O'Hagan, *Angew. Chem.*, 2009, 121, 5565-5568.
14. L. Hunter, K. A. Jolliffe, M. J. T. Jordan, P. Jensen and R. B. Macquart, *Chem. Eur. J.*, 2011, 17, 2340-2343.
15. F. Scheidt, P. Selter, N. Santschi, M. C. Holland, D. V. Dudenko, C. Daniliuc, C. Meck-Lichtenfeld, M. R. Hansen and R. Gilmour, *Chem. Eur. J.*, 2017, 23, 6142-6149.
16. N. E. J. Gooseman, D. O'Hagan, M. J. G. Peach, A. M. Z. Slawin, D. J. Tozer and R. J. Young, *Angew. Chem.*, 2007, 119, 6008-6012.
17. L. Goodman, H. Gu and V. Pophristic, *J. Phys. Chem. A*, 2005, 109, 1223-1229.
18. D. Y. Buissonneaud, T. van Mourik and D. O'Hagan, *Tetrahedron*, 2010, 66, 2196-2202.
19. F. A. Martins and M. P. Freitas, *Eur. J. Org. Chem.*, 2019, 6401-6406.
20. F. Weinhold, C. R. Landis and E. D. Glendening, *Int. Rev. Phys. Chem.*, 2016, 35, 399-440.

21. F. M. Bickelhaupt and E. J. Baerends, *Angew. Chem. Int. Ed.*, 2003, 42, 4183-4188.

22. P. Su and H. Li, *J. Chem. Phys.*, 2009, 131, 014102.

23. M. Baranac-Stojanović, *RSC Adv.*, 2014, 4, 43834-43838.

24. J. C. R. Thacker and P. L. A. Popelier, *J. Phys. Chem. A*, 2018, 122, 1439-1450.

25. C. R. S. Briggs, M. J. Allen, D. O'Hagan, D. J. Tozer, A. M. Z. Slawin, A. E. Goeta and J. A. K. Howard, *Org. Biomol. Chem.*, 2004, 2, 732-740.

26. C. Tormena, M. P. Freitas, R. Rittner and R. J. Abraham, *Phys. Chem. Chem. Phys.*, 2004, 6, 1152-1156.

27. B. C. Fiorin, E. A. Basso, C. Tormena, R. Rittner and R. J. Abraham, *J. Phys. Chem. A*, 2009, 113, 2906-2913.

28. G. Pattison, *Beilstein J. Org. Chem.*, 2017, 13, 2915-2921.

29. C. Trindle, P. Crum and K. Douglass, *J. Phys. Chem. A*, 2003, 107, 6236-6242.

30. E. Cosimi, N. Trapp, M.-C. Ebert and H. Wennemers, *Chem. Commun.*, 2019, 55, 2253-2256.

31. J. Aleksić, M. Stojanović and M. Baranac-Stojanović, *J. Org. Chem.*, 2015, 80, 10197-10207.

32. E. Bogdan, G. Compain, L. Mtashobya, J.-Y. Le Questel, F. Besseau, N. Galland, B. Linclau and J. Graton, *Chem. Eur. J.*, 2015, 21, 11462-11474.

33. R. A. Cormanich, D. O´Hagan and M. Bühl, *Angew. Chem. Int. Ed.*, 2017, 56, 7867-7870.

34. M. A. Blanco, A. Martín Pendás and E. Francisco, *J. Chem. Theory Comput.*, 2005, 1, 1096-1109.

35. D. Suárez, N. Díaz, E. Francisco and A. Martín Pendás, *ChemPhysChem*, 2018, 19, 973-987.

36. S. Grimme, *WIREs Comput Mol Sci*, 2011, 1, 211-228.

37. A. D. Becke and E. R. Johnson, *J. Chem. Phys.*, 2005, 122, 154104.

38. L. Goerigk and J. R. Reimers, *J. Chem. Theory Comput.*, 2013, 9, 3240-3251.

39. L. Goerigk, C. A. Collyer and J. R. Reimers, *J. Phys. Chem. B*, 2014, 118, 14612-14626.

40. T. Ziegler and A. Rauk, *Theoret. Chim. Acta*, 1977, 46, 1-10.

41. F. M. Bickelhaupt and E. J. Baerends, in *Rev. Comput. Chem.*, John Wiley & Sons, Inc., 2007, DOI: 10.1002/9780470125922.ch1, pp. 1-86.

42. E. Francisco and A. Martín Pendás, in *Non-Covalent Interactions in Quantum Chemistry and Physics*, eds. A. Otero de la Roza and G. A. DiLabio, Elsevier, 2017, DOI: https://doi.org/10.1016/B978-0-12-809835-6.00003-7, pp. 27-64.

43. C. Outeiral, M. A. Vincent, Á. Martín Pendás and P. L. A. Popelier, *Chemical Science*, 2018, 9, 5517-5529.

44. E. F. Pettersen, T. D. Goddard, C. C. Huang, G. S. Couch, D. M. Greenblatt, E. C. Meng and T. E. Ferrin, *J Comput Chem.*, 2004, 25, 1605-1612.

45. F. Neese, *WIREs Comput Mol Sci*, 2012, 2, 73-78.

46. S. Grimme, A. Hansen, J. G. Brandenburg and C. Bannwarth, *Chem. Rev.*, 2016, 116, 5105-5154.

47. D. G. Liakos, M. Sparta, M. K. Kesharwani, J. M. L. Martin and F. Neese, *J. Chem. Theory Comput.*, 2015, 11, 1525-1539.

48. N. Sauton, D. Lagorce, B. O. Villoutreix and M. A. Miteva, *BMC Bioinformatics*, 2008, 9, 184.

49. J. Wang, W. Wang, P. A. Kollman and D. A. Case, *J Mol Graph Model*, 2006, 25, 247-260.

50. A. V. Marenich, C. J. Cramer and D. G. Truhlar, *J. Phys. Chem. B*, 2009, 113, 6378-6396.

51. C. Thibaudeau, J. Plavec and J. Chattopadhyaya, *J. Org. Chem.*, 1998, 63, 4967-4984.

52. A. M. Pendas and E. Francisco, Unpublished, 2015.

53. S. Grimme, J. Antony, S. Ehrlich and H. Krieg, *J. Chem. Phys.*, 2010, 132, 154104.

54. E. Francisco, D. Menéndez Crespo, A. Costales and Á. Martín Pendás, *J. Comput. Chem.*, 2017, 38, 816-829.

55. J. Pipek and P. G. Mezey, *J. Chem. Phys.*, 1989, 90, 4916-4926.

56. A. Martín Pendás, M. A. Blanco and E. Francisco, *J Comput Chem*, 2009, 30, 98-109.

57. I. Hyla-Kryspin, G. Haufe and S. Grimme, *Chem. Eur. J.*, 2004, 10, 3411-3422.